Thesis for the degree of Doctor of Philosophy
in the Natural Sciences

---

# The Primary Structural Photo-Response of a Bacterial Phytochrome Probed by Serial Femtosecond Crystallography

---

Elin Claesson

UNIVERSITY OF GOTHENBURG

Department of Chemistry and Molecular Biology
Gothenburg, 2020

Thesis for the degree of Doctor of Philosophy
in the Natural Sciences

The Primary Structural Photo-Response of a Bacterial Phytochrome Probed by Serial Femtosecond Crystallography

Elin Claesson

**Cover:** The difference electron density map at 1 ps after light-activation of the PAS-GAF fragment from *Deinococcus radiodurans.*


ISBN 978-91-7833-870-2 (Print)
ISBN 978-91-7833-871-9 (PDF)
Available online at http://hdl.handle.net/2077/64018

Department of Chemistry and Molecular Biology
Division of Biochemistry and Structural Biology
University of Gothenburg
SE-405 30, Göteborg, Sweden
Printed by BrandFactory AB
Göteborg, Sweden, 2020

*"A seed neither fears light nor darkness, but uses both to grow"*
Matshona Dhliwayo

# Abstract

Species across all kingdoms of life rely on the ability to sense different light conditions. Some organisms convert light into chemical energy via the reactions involved in photosynthesis, whereas others use it to trigger cellular signals. The group of proteins that are responsible for light perception are called photoreceptor proteins. Phytochromes are photoreceptors that control diverse physiological responses in plants, algae, fungi and bacteria, through their ability to sense red and far-red light. These proteins absorb light through a bilin cofactor located in the photosensory part of the protein. Changes in the chromophore induce structural rearrangement in the protein and thereby alter its biological activity. Several structural details of the signalling mechanism remain undetermined and require further investigation.

This thesis focuses on revealing the early structural changes upon photoactivation in the bacterial phytochrome from *Deinococcus radiodurans* (*Dr*BphP). Serial femtosecond crystallography (SFX) has been the main method used for our investigations. The papers presented here describe the crystallization strategies that were used preceding data collection at X-ray free electron lasers (XFELs). Structures of the chromophore binding domain (PAS-GAF) from *Dr*BphP were solved in the resting state, and at 1 ps following light-activation. Additional time-resolved diffraction data were collected at 0-2.7 ps, probing the earliest structural changes after photon absorption. The findings reveal that the captured photoresponse involves extended structural rearrangements including both the chromophore and the protein. Two conserved tyrosine residues are proposed to be involved in the earliest signalling on femtosecond time scale. Subsequently, a collective response of the chromophore and the surrounding binding pocket evolve on an early picosecond time scale.

The discoveries have provided insight into the primary molecular mechanism that phytochromes use to convert light signals into structural changes. Such research not only deepens our understanding of how all vegetation on earth function, but could also have applications in agriculture where growth patterns in various crops could be made more effective.

# Publications

This thesis consists of the following research papers:

**PAPER I:** Petra Edlund*, Heikki Takala*, **Elin Claesson**, Léocadie Henry, Robert Dods, Heli Lehtivuori, Matthijs Panman, Kanupriya Pande, Thomas White, Takanori Nakane, Oskar Berntsson, Emil Gustavsson, Petra Båth, Vaibhav Modi, Shatabdi Roy-Chowdhury, James Zook, Peter Berntsen, Suraj Pandey, Ishwor Poudyal, Jason Tenboer, Christopher Kupitz, Anton Barty, Petra Fromme, Jake D. Koralek, Tomoyuki Tanaka, John Spence, Mengning Liang, Mark S. Hunter, Sebastien Boutet, Eriko Nango, Keith Moffat, Gerrit Groenhof, Janne Ihalainen, Emina A. Stojković, Marius Schmidt and Sebastian Westenhoff. * These authors contributed equally. *The room temperature crystal structure of a bacterial phytochrome determined by serial femtosecond crystallography.* Scientific Reports (2016) doi.org/10.1038/srep35279

**PAPER II:** **Elin Claesson***, Weixiao Yuan Wahlgren*, Heikki Takala*, Suraj Pandey, Leticia Castillon, Valentyna Kuznetsova, Léocadie Henry, Matthijs Panman, Melissa Carrillo, Joachim Kübel, Rahul Nanekar, Linnea Isaksson, Amke Nimmrich, Andrea Cellini, Dmitry Morozov, Michał Maj, Moona Kurttila, Robert Bosman, Eriko Nango, Rie Tanaka, Tomoyuki Tanaka, Luo Fangjia, So Iwata, Shigeki Owada, Keith Moffat, Gerrit Groenhof, Emina A. Stojkovic,Janne A. Ihalainen, Marius Schmidt and Sebastian Westenhoff. * These authors contributed equally. *The primary structural photoresponse of phytochromeproteins captured by a femtosecond X-ray laser*. eLife (2020) doi: 10.7554/eLife.53514

**PAPER III:** **Elin Claesson**, Suraj Pandey, Joachim Kübel, Weixiao Yuan Wahlgren, Heikki Takala, Matthijs Panman, Cecilia Wickstrand, Manoop Chenchiliyan, Leticia Castillon, Amke Nimmrich, Valentyna Kuznetsova, Léocadie Henry, Andrea Cellini, Michał Maj, Eriko Nango, Rie Tanaka, Tomoyuki Tanaka, Luo Fangjia, So Iwata, Shigeki Owada, Emina A. Stojkovic, Janne A. Ihalainen, , Marius Schmidt and Sebastian Westenhoff. *Ultrafast structural changes in a bacterial phytochrome resolved by serial femtosecond crystallography*. Manuscript (2020)

**PAPER IV:** Juan C. Sanchez, Melissa Carrillo, Suraj Pandey, Moraima Noda, Luis Aldama, Denisse Feliz, **Elin Claesson**, Weixiao Yuan Wahlgren, Gregory Tracy, Phu Duong, Angela C. Nugent, Andrew Field, Vukica Srajer, Christopher Kupitz, So Iwata, Eriko Nango, Rie Tanaka, Tomoyuki Tanaka, Luo Fangjia, Kensuke Tono, Shigeki Owada, Sebastian Westenhoff, Marius Schmidt and Emina A. Stojkovic. *High-resolution crystal structures of a myxobacterial phytochrome at cryo and room temperatures*. Structural Dynamics (2019) doi:10.1063/1.5120527

Related papers that I have co-authored but that are not included in this thesis:

**PAPER V:** Nicole C. Woitowich, Andrei S. Halavaty, Patricia Waltz, Christopher Kupitz, Joseph Valera, Gregory Tracy, Kevin D. Gallagher, **Elin Claesson**, Takanori Nakane, Suraj Pandey, Garrett Nelson, Rie Tanaka, Eriko Nango, Eiichi Mizohata, Shigeki Owada, Kensure Tono, Yasumasa Joti, Angela C. Nugent, Hardik Patel, Ayesha Mapara, James Hopkins, Phu Duong, Dorina Bizhga, Svetlana E. Kovaleva, Rachael St. Peter, Cynthia N. Hernandez, Wesley B. Ozarowski, Shatabdi Roy-Chowdhuri, Jay-How Yang, Petra Edlund, Heikki Takala, Janne Ihalainen, Jennifer Brayshaw, Tyler Norwood, Ishwor Poudyal, Petra Fromme, John C. H. Spence, Keith Moffat, Sebastian Westenhoff, Marius Schmidt and Emina A. Stojkovic. *Structural basis for light control of cell development revealed by crystal structures of a myxobacterial phytochrome.* IUCrJ (2018) doi:10.1107/S2052252518010631

**PAPER VI:** Robert Dods, Petra Båth, David Arnlund, Kenneth R. Beyerlein, Garrett Nelson, Mengling Liang, Rajiv Harimoorthy, Peter Berntsen, Erik Malmerberg, Linda Johansson, Rebecka Andersson, Robert Bosman, Sergio Carbajo, **Elin Claesson**, Chelsie E. Conrad, Peter Dahl, Greger Hammarin, Mark S. Hunter, Chufeng Li, Stella Lisova, Despina Milathianaki, Joseph Robinson, Cecilia Safari, Amit Sharma, Garth Williams, Cecilia Wickstrand, Oleksandr Yefanov, Jan Davidsson, Daniel P. DePonte, Anton Barty, Gisela Brändén and Richard Neutze. *From Macrocrystals to Microcrystals: A Strategy for Membrane Protein Serial Crystallography.* Structure (2017) doi:10.1016/j.str.2017.07.002.

**PAPER VII:** Robert Dods, Petra Båth, David Arnlund, Hoi Ling Luk, Robert Bosman, Kenneth R Beyerlein, Garrett Nelson, Mengling Liang, Despina Milathianaki, Joseph Robinson, Rajiv Harimoorthy, Peter Berntsen, Erik Malmerberg, Linda Johansson, Rebecka Andersson, Sergio Carbajo, **Elin Claesson**, Chelsie E. Conrad, Peter Dahl, Greger Hammarin, Mark S. Hunter, Chufeng Li, Stella Lisova, Antoine Royant, Cecilia Safari, Amit Sharma, Garth J. Williams, Cecilia Wickstrand, Oleksandr Yefanov, Jan Davidsson, Daniel P. Deponte, Sebastien Boutet, Anton Barty, Gerrit Groenhof, Gisela Brändén and Richard Neutze. *Ultrafast structural changes in photosynthetic reaction centres visualized using XFEL radiation.* Submitted Manuscript (2020)

# Contribution report

**PAPER I:** I purified the protein and optimized the batch crystallization conditions. I participated in data collection at LCLS and the refinement of the SFX structures. I wrote parts of the paper and made figures.

**PAPER II:** I contributed to a great extent in the planning and preparation of the experiment. I purified and crystallized the protein and collected data at SACLA. I was highly involved in refinement of dark and light structures and calculation and analysis of difference electron density maps. I wrote parts of the paper and made figures.

**PAPER III:** I was highly involved in the planning and preparation of the experiment. I purified the protein and made microcrystals. I collected the data at SACLA and performed the analysis of difference electron density maps and 1D plots. I wrote the paper and made figures.

**PAPER IV:** I contributed to planning the experiment, collected the data at SACLA, and commented on the paper.

# Abbreviations

Here follows a list of the different abbreviations used in this thesis.

| | |
|---|---|
| **BLUF** | **B**lue-**L**ight **U**sing **F**lavin |
| **BphP** | **B**acterial **ph**ytochrome **P**rotein |
| **CA** | **C**atalytic **A**TP binding |
| **CBD** | **C**hromophore **B**inding **D**omain |
| **CCD** | **C**harge **C**oupled **D**evice |
| **Cryo-EM** | **Cryo**genic-**E**lectron **M**icroscopy |
| **CSPAD** | **C**ornell-**S**LAC **P**ixel **A**rray **D**etector |
| **DHp** | **D**imerization and **H**isitidine **p**hosphotransfer |
| **EMR** | **E**lectro**M**agnetic **R**adiation |
| **ESRF** | **E**uropean **S**ynchrotron **R**aditation **F**acility |
| **GAF** | c**G**MP-specific phosphodiesterase-**A**denylyl cyclase-**F**hlA |
| **GDVN** | **G**as **D**ynamic **V**irtual **N**ozzle |
| **HK** | **H**istidine **K**inase |
| **HPLC** | **H**igh **P**erformance **L**iquid **C**hromatography |
| **IMAC** | **I**mmobilized **M**etal **A**ffinity **C**hromatography |
| **LCLS** | **L**inac **C**oherent **L**ight **S**ource |
| **LCP** | **L**ipidic **C**ubic **P**hase |
| **LOV** | **L**ight-**O**xygen-**V**oltage |
| **MPCCD** | **M**ulti-**P**rot **C**harge-**C**oupled **D**evice |
| **NTE** | **N**-**T**erminal **E**xtension |
| **PAS** | c**P**er-**A**rnt-**S**im |
| **PCC** | **P**earson **C**orrelation **C**oefficient |
| **PHY** | c**Phy**tochrome-specific |
| **PW** | **P**yrrole **W**ater |
| **PYP** | **P**hotoactive **Y**ellow **P**rotein |
| **RR** | **R**esponse **R**egulator |
| **SACLA** | **S**Pring-8 **A**ngstrom **C**ompact free electron **LA**ser |
| **SAXS** | **S**mall **A**ngle **X**-ray **S**cattering |
| **SEC** | **S**ize-**E**xclusion **C**hromatography |
| **SDS-PAGE** | **S**odium **D**odecyl **S**ulfate–**P**oly**A**crylamide **G**el **E**lectrophoresis |

| | |
|---|---|
| **SFX** | **S**erial **F**emtosecond crystallography |
| **SNR** | **S**ignal-to-**N**oise **R**atio |
| **STEM** | **S**canning **T**ransmission **E**lectron **M**icroscope |
| **XFEL** | **X**-ray **F**ree-**E**lectron **L**aser |
| *Dr* | *Deinococcus radiodurans* |
| *E. coli* | *Escherichia coli* |
| *Sa* | *Stigmatella aurantiaca* |

# Contents

# Chapter 1

# Introduction

## 1.1 Light

We experience waves in various aspects in our everyday life. When listening to our favourite song on the radio, when having an X-ray scan at the hospital or getting a nice tan (i.e. sunburn) in summer. All these examples involve electromagnetic waves. Electromagnetic radiation (EMR) is a form of energy carried by photons, which are particles without mass travelling at the speed of light. Depending on the characteristics of different electromagnetic waves such as the wavelength or frequency, they can be grouped in the electromagnetic spectrum [1] (see Fig. 1.1).

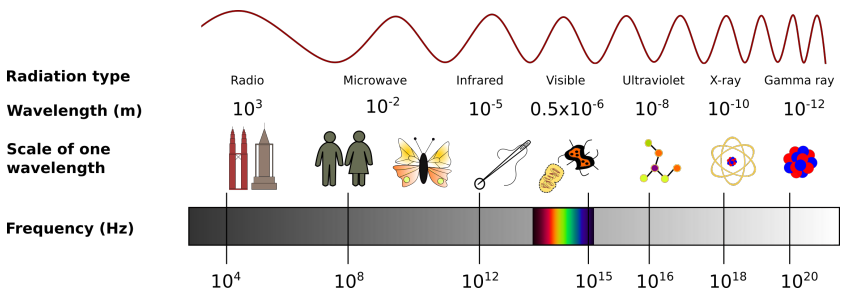


**Figure 1.1: Electromagnetic radiation.** An overview of different types of electromagnetic radiation, their wavelengths, frequencies and relative scales. The spectrum includes radio waves (longer wavelengths), microwaves, infrared radiation (IR), visible light, ultraviolet (UV), X-rays and gamma rays (shorter wavelengths).

The sun emits different types of electromagnetic radiation and the part which reaches the Earth is called solar radiation. Visible light (380-740 nm) is part of the solar radiation [2] and through evolution organisms have

evolved to respond to various light conditions. Photosynthetic organisms can covert light energy into chemical energy which is used for a multitude of cellular processes. Furthermore, light acts as an external trigger for organisms to send cellular signals and non-photosynthetic organisms also depend on light to be able to interact with the world [3].

## 1.2 Photoreceptors

Organisms are able to respond to their environmental conditions in numerous ways through different sensory receptors. Various stimuli are detected by specific ligands embedded in the sensory receptors. Changes in the properties of the ligand further triggers a response in the receptor that results in modulation of its functional state. Receptor proteins that respond to changes in light conditions are called photosensory proteins. These proteins are further subdivided according to which ligand, or chromophore, the protein binds and what wavelengths it responds to. Examples of different types of photoreceptors are rhodopsins, photoactive yellow proteins (PYPs), light-oxygen-voltage (LOV) proteins, cryptochromes, blue-light using flavin (BLUF) proteins and phytochromes [4]. Although the aforementioned photoreceptors exhibit different properties regarding light absorption, structure and biological responses, they utilize only four types of chromophores. It is therefore not surprising one observes emerging themes amongst these photoreceptors in terms of the molecular mechanism of photoactivation.

Generally, the photochemical cycle of the photoreceptor is initiated with the absorption of a photon by the chromophore. On a picosecond time scale, the excited chromophore relaxes to an electronic ground state with a different geometry and/or oxidation state. Examples of changes in the local environment of the chromophore caused by photon absorption are isomerization [5] and proton/electron transfer [6]. These initial local photochemical events in the chromophore triggers consequential structural evolution in the protein, resulting in formation of the signalling state. In the signalling state, the protein transfers the signal to subsequent components in the signal-transduction chain, resulting in a cellular response [4] (see Fig. 1.2).

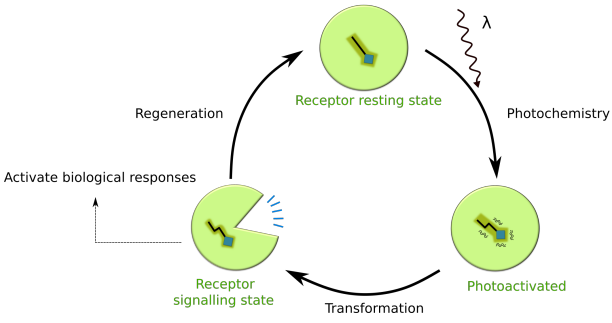


**Figure 1.2: General description of photoreceptor function.** Photoactivation of the chromophore is induced by photon absorption (oscillating arrow). The generated changes in the chromophore propagates through the protein, resulting in the signalling state of the protein which further triggers a cellular response. The receptor resting state is eventually regenerated in which the protein once again is accessible to stimuli.

## 1.3 Phytochromes

Phytochromes are photoreceptor proteins that sense light in the red and far-red region of the visible spectra [3]. They play an important role in bacteria, algae, fungi and plants regarding the organism's ability to respond and acclimatize to the surrounding light conditions [7]. For example, phytochromes are involved in the regulation of developmental biological processes such as shade avoidance and seed germination [8]. The regulatory function of the protein is achieved by the reversible switching between two metastable states; the Pr state (red absorbing) and the Pfr state (far-red absorbing)(see Fig. 1.3 A). Transition between the two different states of the protein is, for example, guiding plants to grow from the shadow (high far-red:red ratio) towards the light (low far-red:red ratio). Most phytochromes have the Pr as their resting state and are called canonical phytochromes. Although, phytochromes that relax to the Pfr state exist and are called bathy phytochromes [9]. Phytochromes were first found in plants [10, 11] but were later also discovered in fungi [12] and different types of bacteria [13, 14]. However, there are both functional and structural differences between prokaryotic and eukaryotic phytochromes.

Phytochromes are soluble proteins that exists as homodimers. The structural composition of a prototypical phytochrome consists of an N-terminal

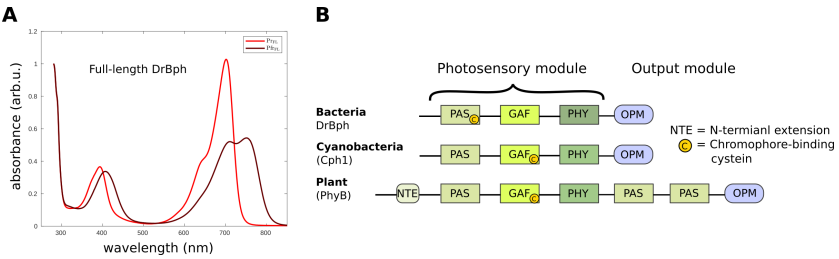


**Figure 1.3: Spectral properties and domain architecture of phytochromes.** A.) Absorption spectra of the two metastable states (Pr (red absorbing) state and Pfr (far-red absorbing state)) of the full-length bacterial phytochrome from *Deinococcus radiodurans*. B.) Overview of variations in domain composition of different phytochromes.

photosensory module, which binds the chromophore and responds to light, and a C-terminal output module which translates the signal further to downstream signalling pathways. The photosensory core consists of a PAS (Per/Arnt/Sim), GAF (cGMP phosphodiesterase/ adenylyl cyclase/FhlA) and PHY (phytochrome-specific) domain. The chromophore utilized by bacteria is biliverdin, which is covalently bonded to a cysteine in the PAS domain. Phytochromes in cyanobacteria and plants bind different types of chromophores, phycocyanobilin and phytochromobilin respectively, which are both bound to the GAF domain. The output domain for bacteria and cyanobacteria is usually a histidine kinase (HK) domain. The HK domain consists of two subdomains: a Catalytic ATP-binding (CA) domain and a Dimerization Histidine phosphotransfer (DHp) domain. Plant phytochromes have an N-terminal extension (NTE) and two extra PAS domains. The output domain of plant phytochromes is homologous to the prokaryotic histidine kinase domain but it lacks a conserved phosphoryl group-accepting histidine [15]. In summary, the photosensory module is very similar between organisms whereas the chromophore and the output module vary to a larger extent (see Fig. 1.3 B). Preservation of the photosensory core allows us to learn from simpler systems and draw parallels across different kingdoms.

## 1.4 Bacteriophytochromes

In contrast to plant phytochromes (Phys) where several of the physiological functions have been characterized [8], the role of bacteriophytochrome (BphPs) from non-photosynthetic bacteria still remains largely unknown. However, several discoveries have been made concerning the signalling mechanism of these model systems. BphPs are involved in a two-component phosphorylation system between the phytochrome and a response regulator protein (RR) [3]. The C-terminal HK domain first auto-phosphorylates, which is followed by phosphotransfer between the kinase domain and the response RR. The RR further controls transcription of light responsive genes in accordance to its phosphorylation state [16] (see Fig. 1.4). Owing to the greater structural complexity of plant phytochromes, these participate in more extended signalling cascades than their prokaryotic counterparts [17]. The photoreaction, which ultimately results in a cellular response, is initiated by excitation of the chromophore. The chromophore utilized by BphPs is as previously mentioned biliverdin, which is an open tetra-pyrrole chain derived from oxidative degradation of the heme cofactor. The four rings A-D constitute a conjugated double bond system responsible for photon absorption [18] (See Fig. 1.4).

### 1.4.1 The photocycle of BphPs

Bacterial phytochromes are the least complex systems regarding photoactivation and number of intermediates formed during Pr/Pfr photoconversion. Different spectroscopic methods have been used to investigate the photocycle of phytochromes from bacteria and cyanobacteria. Three intermediates are formed during Pr to Pfr photoactivation; Lumi-R, Meta-Ra and Meta-Rc (See Fig. 1.6). Lumi-R forms within picoseconds [5,19–21] and is thereafter converted into Meta-Ra on a microsecond time scale. Meta-Ra proceeds via Meta-Rc to form the final photoproduct, Pfr, within milliseconds. Deprotonation/reprotonation events occur in the later stages of the photocycle for canonical phytochromes [22, 23]. However, in a recent study on the bacteriophytochrome from *Deinococcus radiodurans (Dr*BphP), the Meta-Ra and Meta-Rc intermediates could not be distinguished [24]. The Pr-state

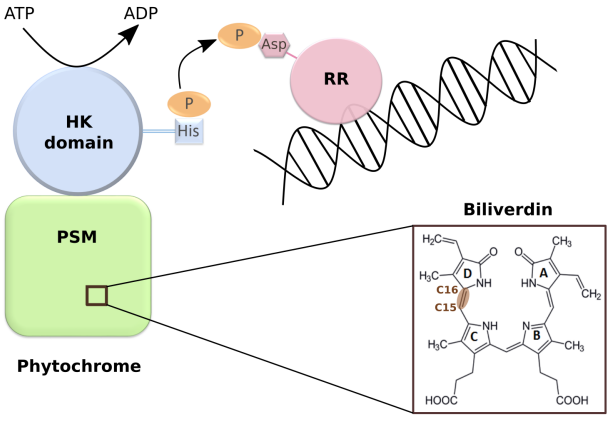


**Figure 1.4: Phytochrome regulation.** Phytochromes are part of a two-component regulatory system. Auto-phosphorylation of a histidine residue in the HK domain leads to phosphorylation of an aspartate residue in the response regulator protein (RR). The RR further mediates a cell response by interacting with the DNA, which commonly results in increased transcription levels of target genes. The chromophore in bacterial phytochromes is biliverdin which is located in the photosensory module (PSM) of the protein. A chemical illustration of the biliverdin is represented in the square, with the rings A-D marked in bold letters. The C15=C16 double bond, around which the D-ring isomerizes, is highlighted in the figure.

is spontaneously regenerated through thermal dark reversion but this process can also be accelerated with illumination of far-red light [25–27]. For the latter case, two intermediates are formed called Lumi-F and Meta-F. The primary step in Pr-to-Pfr photoconversion is considered to involve Z-to-E isomerization, and vise versa, of the chromophore D-ring around the $C_{15}$=$C_{16}$ double bond [24, 27–32].

### 1.4.2 Structural features of BphPs

It is well-known that the structure of a protein is closely related to its function. The discovery of bacteriophytochromes facilitated the production, and therefore the structural investigation, of phytochrome proteins. One of the most successful methods used for solving the three-dimensional structure of proteins is X-ray crystallography. The first solved crystal structure of a phytochrome was the PAS-GAF fragment of the bacterial phytochrome from *Deinococcus radiodurans* [33]. This structure provided insight into the spacial position of biliverdin within the protein and the importance of many conserved residues could be explained structurally by their location within the protein. Henceforth, many crystal structures of varying phytochrome domains from different organisms have been solved [32, 34–43].

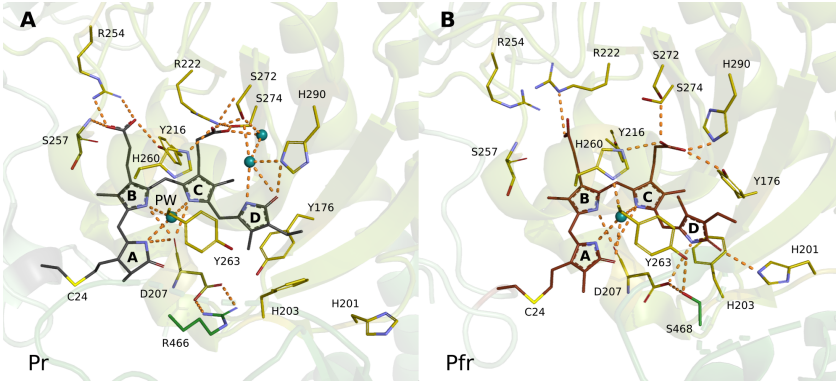


**Figure 1.5: An overview of the chromophore binding pocket in Pr and Pfr** A.) The chromophore binding pocket of *Dr*BphP in the Pr-state (pdb:4q0j). Hydrogen bonds are marked with orange dashed lines and selected waters are shown as blue spheres. The PHY-tongue interaction partner R466 is shown in dark green. B.) The same view shown for *Dr*BphP in the Pfr-state (pdb:5c5k). The new PHY-tongue interaction partner S468 is colored dark green.

In *Dr*BphP, biliverdin is covalently attached to the protein via a thioether linkage between the A-ring and a cysteine residue in the PAS-domain (see Fig. 1.5 A). The chromophore binding pocket, in contrast, is positioned within the GAF-domain where additional interactions between biliverdin and the protein are formed through non-covalent bonds and hydrophobic interactions. The A-to-C rings of biliverdin are co-planar whereas the D-ring is rotated out of this plane. Furthermore, the packing around the D-ring is relatively sparse, creating a small cavity which allows for isomerization around the $C_{15}$=$C_{16}$ bond to occur. Several conserved residues among the phytochrome family are located within a short distance of the chromophore and take part in various protein-chromophore interactions. The A-ring is closely positioned to the highly conserved DIP-motif ($Asp_{207}$-$Ile_{208}$-$Pro_{209}$) and the backbone oxygen of $Asp_{207}$ forms hydrogen bonds with rings A-C of the chromophore (the numbering corresponds to the phytochrome found in *Deinococcus radiodurans*). The B-ring propionate group interacts with $Arg_{254}$, $Ser_{257}$ and $Tyr_{216}$, whereas the C-ring propionate binds to $His_{260}$, $Ser_{272}$ and $Ser_{274}$. The D-ring is stabilized by a hydrogen bond between the carbonyl group and $His_{290}$ and the surrounding water network. The cavity around the D-ring is partly formed by the residues $Tyr_{176}$, $Tyr_{263}$ and $Phe_{203}$. Several conserved waters have been identified, for example the so-called pyrrole water (PW) which is found in all phytochrome structures. This water is located in the middle of the chromophore and interacts with the nitrogen atoms of ring A-C.

The structures of the full photosensory module (PAS-GAF-PHY) revealed that the PHY-domain extends from the GAF-domain through a single long helix (see Fig. 1.6). A surprising finding was a region (often referred to as the tongue region) that reaches back towards the chromophore binding pocket and shields the chromophore from solvent exposure. The tongue region includes the highly conserved $_{465}$PRXSF$_{469}$ motif. In the Pr state of *Dr*BphP, the most direct interaction of the chromophore binding pocket and the tongue region is a salt-bridge formed between $Asp_{207}$ and $Arg_{466}$ [37]. A full-length structure with the HK domains attached, however, is not yet determined to an atomic resolution.

### 1.4.3 Signal transduction in phytochromes

The complete photosensory module from *Dr*BphP has been solved in both the Pr- and Pfr-state [32, 37]. Structural changes connected to the photoactivation mechanism have thus been identified. The D-ring was found to be flipped from a ZZZssa confirmation in Pr to a ZZEssa conformation in Pfr [32], confirming the proposed isomerization of the $C_{15}$=$C_{16}$ double bond. Associated changes with the two different chromophore conformations were also observed within the chromophore-binding pocket (see Fig. 1.5 B). The conformation of several of the above mentioned amino acids such as $Tyr_{176}$, $His_{290}$, $Tyr_{263}$, $Phe_{203}$ adopted new conformations in the Pfr structure. The B- and C-ring propionate groups both rearrange and switch interaction partners during the Pr/Pfr photoconversion. In addition, the tongue region refolds during the photoswitching, from a $\beta$-sheet in Pr to an $\alpha$-helix and a loop in Pfr (See Fig. 1.6). The salt bridge between $Asp_{207}$ and $Arg_{466}$ was therefore broken and new bonds were formed between $Asp_{207}$, $Tyr_{263}$ and $Ser_{468}$ [37]. $Asp_{207}$ and $Arg_{466}$ were furthermore suggested to play an important role in Lumi-R formation where they would form a hydrogen-bonding cluster with the NH and C=O groups of the D-ring [24]. Refolding of the tongue region also causes the PHY-domains, that are close in distance in the Pr-state, to move apart by ∼3 nm in the Pfr-state.

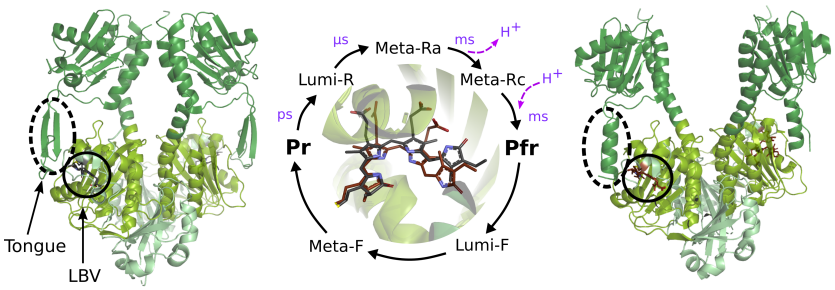


**Figure 1.6: Phytochrome signalling** The structures of Pr (left, pdb:4O0P) and Pfr (right, pdb:4O01) of the full photosensory core are shown. The PAS,GAF and PHY domains are colored light green, olive and dark green, respectively. The photocycle of canonical phytochromes is illustrated around the biliverdin chromophore (LBV) conformations in Pr (grey) and Pfr (brown).

Attempts to understand the full signal transduction chain in phytochromes have been made by studying the full-length protein fragment.

Examples are the works performed using scanning transmission electron microscopy [44] and single particle Cryo-EM methods [45]. Separation of the PHY-domains were supported and large scale repositioning of the kinase domains relative to the photosensory core were observed. However, the resolution of the HK domains was low, suggesting high flexibility in these domains. Small-Angle X-ray Scattering (SAXS) experiments were also performed to investigate the global changes occurring in phytochromes during photoactivation. In *Dr*BphP the global structural changes were found to occur within a few milliseconds. In the full-length protein, the HK output domains did not separate, as was observed for the PHY-domains in the photosensory module. Instead, the data indicated that a rotational motion had occurred, resulting in a twist of the output domains with respect to the chromophore-binding domains [46]. A rotation of the HKs would further induce a different binding geometry of the subdomains, CA domains and DHp helices, whose orientation have been proven important for HK activity [47].

A mechanism emerges from the above considerations: the local changes in the chromophore binding pocket initiate a refold of the PHY-tongue. The structural changes within the PHY domains further affect the orientation of the HK domains. Subsequently the kinase activity is modified and results in a shifted equilibrium of the Pr/Pfr state. However, high resolution structures of the full-length protein are needed for a more detailed view of the global signalling mechanism in phytochromes.

## 1.5 Scope of this thesis

Structures of the photosensory core in Pr- and Pfr-states have been solved and the photocycle for several BphPs have been determined. However, structural changes that are coupled to the intermediate states formed during photoconversion, are still poorly understood. This thesis is aimed at the investigation of the molecular mechanism used by phytochromes during photoactivation. The initial events following photon absorption have been the central target of our investigations. The main technique used for this work is serial femtosecond crystallography (SFX), which is one of the most suitable techniques to use when studying structural changes on short time scales. This technique requires microcrystals which have been successfully produced for the PAS-GAF fragment. The full-length phytochrome protein does not form

well-diffracting crystals and investigation of the global structural changes calls for alternative methods. Therefore a project was started on the full-length phytochrome from *Deinococcus radiodurans* using the advantages of single particle Cryo-EM.

**Paper I** presents two alternative procedures to produce microcrystals of the PAS-GAF fragment from *Deinococcus radiodurans* for SFX experiments. The paper further includes the first room temperature crystal structure of the same protein fragment in its dark state. In **paper II** time-resolved crystallography data were collected at 1 and 10 ps, elucidating the early structural changes after photoactivation. **Paper III** aims at tracking the changes leading up to our previously solved structure at 1 ps. Data were collected at time points spanning from 0-2.7 ps. The results generated information about the sequence of structural changes that occur as a response to photon absorption. In **paper IV** three crystal structures of the full photosensory core of a phytochrome from *Stigmatella aurantiaca* were solved. This paper establishes the framework for future studies of the full photosensory core and later stages of the photocycle of phytochromes.

The methods and results related to **paper I-IV** are described in chapter 2-5. Chapter 6 presents the results obtained from the Cryo-EM project on the full-length phytochrome from *Deinococcus radiodurans*. Chapter 7 includes a summary of my work and an outlook for future research on phytochromes.

# Chapter 2

# Sample preparation for SFX experiments

Most of the projects upon which this thesis is based are focused on the structural characterization of the bacterial phytochrome from *Deinococcus radiodurans*. Chapter 2 includes a description of the methods used for sample preparation along with a short summary of their applicability in the phytochrome project.

## 2.1 Protein production

Many methods used for structure determination require large quantities of highly pure protein. Hundreds of milligrams of protein are sometimes necessary to obtain a SFX data set of sufficient quality [48]. Direct extraction of the protein sample from the original source often does not meet the stringent requirements. Fortunately, the use of recombinant protein expression allows us to overcome the obstacle of generating large amounts of protein sample [49, 50]. In this approach, the gene encoding the protein of interest is cloned into a DNA-vector designed for expression purposes. Transformation of the exogenous DNA into a host system such as *Escherichia coli* (*E. coli*), allows for high amounts of protein to be expressed in a short time [51].

The use of *E. coli* as a host system is favourable when working with prokaryotic proteins due to the short generation time and high similarity of cell architecture to the natural source. The common T7 expression host BL21 (DE3), carries a gene encoding the phage T7 RNA polymerase within its chromosomal DNA [51, 52]. This gene is under control of the

lac promoter, which in turn is regulated by the lac repressor. Upon induction with Isopropyl $\beta$-D-1-thiogalactopyranoside (IPTG), the repressor is released and T7 RNA polymerase is expressed. The T7 promoter within the DNA-vector is recognized by the T7 RNA polymerase and binding allows for transcription of target genes located downstream of the promoter site.

When phytochromes are expressed in nature, the bilin chromophore is abundant within the cell environment. Biliverdin is a product of the degradation of heme by the enzyme heme oxygenase. However, when phytochromes are recombinantly expressed, the chromophore must be provided externally. Phytochromes can be expressed as holoproteins as a result of co-transformation with a plasmid carrying the heme oxygenase gene [53]. Alternatively, the protein can be expressed as apoprotein whereupon the chromophore is added at a later step during the purification scheme [25, 54].

The *Dr*BphP fragments were expressed as apoproteins in the pET21b(+) vector, using the BL21(DE3) cell strain as a host system. The pET21b(+) vector is a T7 promoter based system and contains a C-terminal 6xhistidine tag. Cells were cultured in LB-media at 37°C to an $OD_{600}$ of 0.6-0.8. Protein expression was induced with IPTG (1 mM) and cultured overnight at a reduced temperature (28°C).

## 2.2 Protein purification

Following protein production, the target protein has to be collected from the cells and further separated from other macro molecules. The initial steps during the purification of over-expressed proteins involve cell breakage followed by centrifugation. These steps are performed to extract the proteins from the cells and separate them from cell debris. There are several strategies that can be applied to break cells, including the use of chemicals or external force (such as high pressure operating systems) [55]. Protein purification commonly proceeds via several steps of chromatography where proteins are separated according to their different properties [56]. The principle of column chromatography is based on the usage of a stationary phase and a mobile phase. The column is packed with the stationary phase consisting of a resin in a buffer solution. The mobile phase, comprising of a diverse number of macromolecules, is passed over the column either by gravitation or an automated liquid chromatography system [57, 58]. Macromolecules

will be separated due to their interaction with the stationary phase, which depend on their specific properties. Recombinant protein expression enables the addition of specific tags to the protein sequence. A polyhistidine tag can be added to the N- or C-terminus of the protein, an approach exploited in immobilized metal affinity chromatography (IMAC). In $Ni^{2+}$-affinity chromatography the $Ni^{2+}$-ions are bound to the resin in the stationary phase. As the mobile phase travels over the column, the His-tagged proteins with high affinity for $Ni^{2+}$-ions bind the resin, whereas other macromolecules elute from the column during washes with buffer. The bound proteins can finally be eluted with an increased concentration of imidazole, which is structurally similar to histidine and therefore competes for the $Ni^{2+}$-ions [59, 60].

Proteins can be separated by several different properties, for example according to their size. In size-exclusion chromatography (SEC) the column is packed with a matrix consisting of gel beads, which contain differently sized pores. Large molecules travel outside the beads and thus have shorter retention times and elute first. Small molecules will enter the pores in the beads and therefore have longer retention times and elute later [57]. To improve purity of the sample several purification steps can be combined. However, as the purification procedure expands there is an increased risk of sample loss and protein degradation/instability.

In the work included in this thesis, cells were lysed using the high pressure homogenizer EmulsiFlex -C3 (Avestin). The biliverdin chromophore was added after the lysis step (>10x molar excess) and incubated with the protein overnight at 4°C. All steps following biliverdin incorporation were carried out under green lights to keep the protein stable within the Pr-state. The protein was purified with $Ni^{2+}$-affinity (HisTrap GE healthcare) and size-exclusion chromatography (HiLoad 26/600 Superdex 200 prep grade GE Healthcare). The purified protein was concentrated to 30 mg/ml in 20mM Tris buffer at pH 8.

## 2.3 Confirming protein functionality

Following protein purification, the purity, quantity and functionality of the sample have to be determined. The purity of the protein sample is often analyzed by the gel electrophoresis method sodium dodecyl sulfate–polyacrylamide gel electrophoresis (SDS-PAGE), where proteins are separated according to their size [58]. A single band at the expected molecular weight indicate a pure sample containing the target protein.

Absorption spectroscopy can be used to identify and quantify different molecules based on their electronic structure. The concentration of proteins can be determined through the Beer-Lambert law ($A_{280} = \epsilon cl$). The absorption value at 280 nm ($A_{280}$) corresponds to the absorption of aromatic amino acids and the $\epsilon$ value is the molar extinction coefficient for a certain molecule at a certain wavelength [58]. Since phytochromes can be photoswitched, the functionality of the protein can be explored by recording absorption spectra after illumination with red (660 nm) and far-red light (780 nm), respectively.

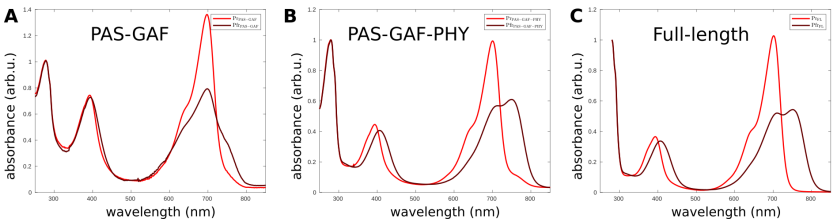


**Figure 2.1: Phytochrome absorption spectra**. Absorption spectra of the A.) PAS-GAF fragment B.) PAS-GAF-PHY fragment and C.) Full-length of the phytochrome from *Dr*BphP in Pr(red) and Pfr (far-red) state.

The UV-visible absorption spectra of different phytochrome fragments from *Dr*BphP is shown in figure 2.1. As demonstrated in the spectra and concluded in previous studies [39, 61], the PAS-GAF fragment does not preserve the spectral integrity of the Pfr state of the full-length protein. Indicating that the PHY domains are required for proper photo-conversion and conformational stability. The ratio between $A_{700}/A_{280}$ differs between truncated versions [25] and it is important to conclude optimal biliverdin incorporation.

## 2.4 Crystallization

A commonly used technique for protein structure determination is X-ray crystallography, which as implied by the name requires crystals. When protein molecules undergo crystallization, they precipitate out of solution in a controlled manner to be arranged in a repetitive pattern in three dimensions. Small identical units are added together through translational symmetry to build up the whole crystal. These units are called unit cells and are defined by the length of their axes a, b, c and the angles between them $\alpha$, $\beta$, $\gamma$. The unit cell is in turn composed of the asymmetric unit, which is the smallest fraction that can be used to generate the complete unit cell through symmetry operations. There are several ways in which crystal packing can occur and these ways are described by different space groups. The space group of a crystal provides information about the unit cell parameters and the symmetry within the unit cell [62].

A protein crystal is formed when the solubility limit of the protein is exceeded and the protein is enforced into a crystalline state. The crystallization process is illustrated in the phase diagram (see Fig. 2.2). Diverse methods can be used for protein crystallization and one of the most common methods is vapour diffusion. In this method the protein is mixed with a solution that contains a precipitant agent. The droplet with mixed protein and precipitant is enclosed in a sealed chamber together with a reservoir solution, which also contains the precipitant. The precipitant concentration is higher in the reservoir solution and water will evaporate from the droplet to restore equilibrium. This process will eventually lead to supersaturation of the drop and formation of nuclei will occur under perfect conditions. Too high protein and/or precipitant concentration will bring the solution into the precipitation zone, which results in protein precipitation. At too low concentrations, on the other hand, the solution will stay in the undersaturated zone and the protein will remain soluble. Nuclei formation lowers the concentration of free protein in the droplet and the protein concentration eventually reaches the metastable zone. When the solution is in the metastable zone the existent nucleus continue to grow into larger crystals [62]. The crystallization drop can either be placed in a hanging or sitting position within the well [63].

The conditions in which crystals will form is highly specific for a certain protein. Therefore it can be tedious work to screen different crystallization conditions to find the optimal composition which yields well-diffracting

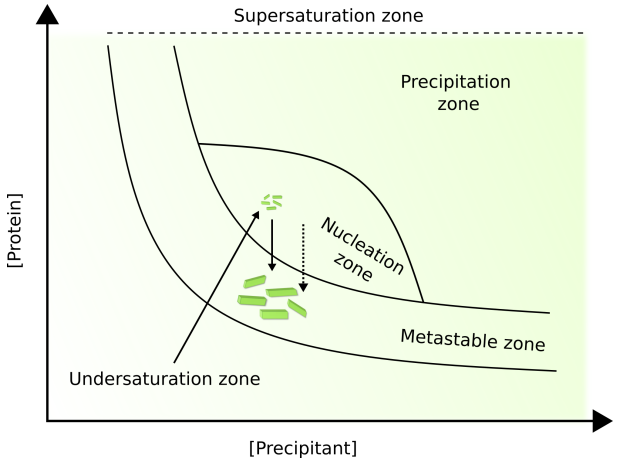


**Figure 2.2: Phase diagram**. Solubility diagram illustrating crystal growth and the relationship between protein and precipitant concentration. Solid arrows describe the procedure of vapour diffusion crystallization whereas the dashed arrow describes batch crystallization.

crystals. Several factors such as protein concentration, buffer composition, purity, temperature, pH, protein:precipitant ratio etc., affect crystal formation. Even after initial crystal conditions have been found, further rounds of screening are typically required to grow large enough crystals of well-diffracting quality for X-ray crystallography experiments.

## 2.5 Micro-crystallization

Contrary to conventional X-ray crystallography, where the typical aim is to grow large macrocrystals, SFX methods demand high amounts of microcrystals. The request for different sizes of crystals are related to the different procedures of data collection, which will be discussed in more detail in chapter 3. The shifted requirements of sample properties have called for development of new crystallization strategies. One approach to produce microcrystals is to mechanically crush up large crystals grown with traditional methods, into smaller crystals. Macrocrystals are then placed in a tube together with seed beads and vortexed until the desired crystal size is

obtained [64]. Cooling in-between rounds of vortex is often applied to reduce heating of the crystals. However, crushing large crystals up into smaller ones generally yields an inhomogeneous crystal size distribution. Although filters can be used to separate crystals of different size, filtering will cause substantial loss of sample and introduce the risk of damaging the crystals.

By growing crystals directly in the correct size range one avoids the disadvantages of crushing and filtering crystals. One method applied for microcrystallization is the batch method. The principle is to start off in the nucleation zone to generate a great amount of nucleation sites [63]. This can be done by either increasing the precipitant and/or protein concentration. The multitude of formed nuclei will cause the protein concentration to rapidly decrease and the existent nuclei will grow into small crystals in the metastable zone (see Fig. 2.2). The protein and reservoir solution is added to a tube and instantly mixed to homogeneity by vortexing. Crystals are further grown under incubation and during this procedure different conditions such as temperature and incubation time have to be optimized. This method can conveniently be combined with seeding, where small microcrystals are introduced as nucleation sites to new crystallization set-ups [65]. Batch crystallization brings the advantage of easy scale up for SFX-experiments and requires little preparation time for sample loading at the experiment.

## 2.6 Crystallization of *Dr*BphP

Both crushing of macrocrystals and batch crystallization methods were applied in the SFX project on the PAS-GAF fragment from *Dr*BphP (**Paper I-III**). Macrocrystals were initially obtained using the hanging drop vapour diffusion method. Protein (20 mg/ml) was mixed together with reservoir solution (67 mM sodium acetate pH 4.95, 3.3% v/v PEG 400, 1 mM DTT and 30% 2-methyl-2,4-pentanediol), in a ratio of 1:1. The drop was equilibrated against reservoir solution (800 $\mu$l) and crystals were formed within 24-48 hours (see Fig. 2.3). The drop size was thereafter scaled up in sitting drop plates to a volume of 20+20 $\mu$l with the protein concentration being adjusted to 25 mg/ml. Crystal solution from a 24 well plate were collected in a microcentrifuge tube and vortexed with two seed beads (Molecular Dimensions). Crystals were crushed repeatedly for 30 s with cooling in-between, until a

crystal size of approximately 10-20 $\mu$m was obtained. Larger crystals could be excluded by filtering with 20 $\mu$m cut-off spin filters (Partec).

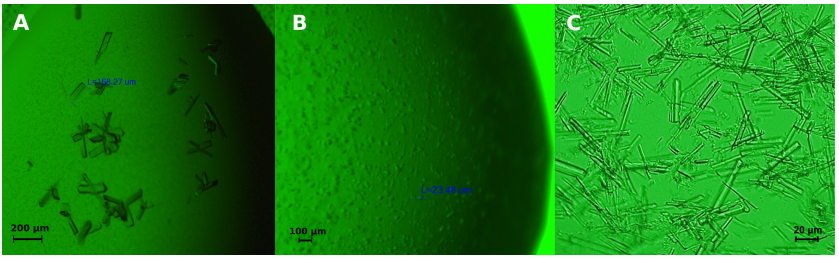


**Figure 2.3: Phytochrome crystals**. A.) Crystals of the PAS-GAF fragment from *Dr*BphP crystallized with the hanging drop method in a drop size of 4 $\mu$l. Crystal size is ~150 $\mu$m. B.) Crystals of the same fragment using the batch crystallization method in a volume of 500 $\mu$l. Crystal size is ~10-30 $\mu$m. C.) Crystals of the same fragment using the batch crystallization method in combination with seeding. Crystal size is ~50-70 $\mu$m

As the project proceeded, the batch crystallization method was tested and further optimized to make crystal growth less onerous and more time effective. Crystal growth in batch mode also entailed a smaller size distribution and a lot less protein crystals were wasted during filtration steps. In batch crystallization, 50 $\mu$l protein (25 mg/ml) was mixed with 450 $\mu$l reservoir solution and immediately vortexed. The solution was incubated at 4°C on a tipping table. Microcrystals of approximately 10-30 $\mu$m appeared within ~36 h (see Fig 2.3).

Seeding was applied as a supplementary step to the initial batch crystallization to increase crystal size. The formed microcrystals were pelleted by centrifugation and 400 $\mu$l of the supernatant were removed. 200 $\mu$l of fresh reservoir solution along with 200 $\mu$l of protein (14 mg/ml) was added to the tube and incubated at room temperature. The crystal size increased and 20-70 $\mu$m long needles formed within 48 h (see Fig. 2.3).

# Chapter 3

# X-ray diffraction and SFX data collection

The molecular mechanism by which phytochrome proteins photoconvert has been the main target of investigation. X-ray crystallography and SFX were the methods used for data collection. The theory and diverse practical aspects of these methods are presented in this chapter followed by the specific settings used for data collection of phytochromes.

## 3.1 X-ray diffraction and data collection

When a crystal is placed in a beam of X-rays, the electrons within the crystal will scatter the incoming waves in different directions. The periodicity within the crystal lattice will cause the scattered waves from all electrons to occur with constructive or destructive interference. If the waves are in phase, as for constructive interference, the signal of the scattered x-rays is amplified. The intensity of coherent scattered X-rays can be observed as Bragg spots (also referred to as reflections) on a detector [62]. A larger crystal contains more scattering elements, thus giving rise to larger constructive interference and higher intensity of the Bragg reflections (see Fig. 3.1). Bragg's law describes the conditions for constructive interference:

$$n\lambda = 2dsin\theta \tag{3.1}$$

where $n$ is a positive integer, $\lambda$ the wavelength of the incoming X-ray, $d$ the distance between two lattice plane and $\theta$ the angle of the incident and scattering X-ray.

X-ray scattering from a protein crystal gives rise to a diffraction pattern consisting of many Bragg reflections. Each Bragg peak (h,k,l) corresponds to diffraction from a set of planes in the crystal defined by Miller indices (hkl). The various intensities and positions of the measured Bragg reflections depend on the atomic content within the unit cell. The intensity of a reflection is proportional to the amount of scatterers and the positions of reflections are related to the arrangement of atoms in three-dimensional space. The real crystal lattice is also represented in reciprocal space and the two lattices are related through a Fourier transform. The criteria for diffraction and the relation between the real and reciprocal space can be described by Edward's sphere (see Fig. 3.1) [66].

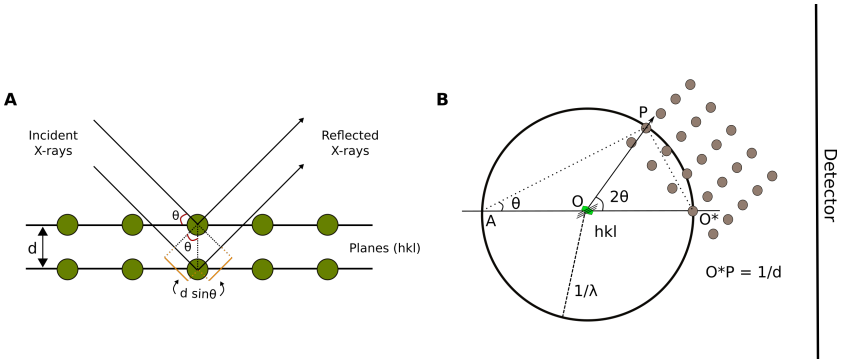


**Figure 3.1: Illustration of Bragg's law and Edwald's sphere**. A.) A description of the geometry used in Bragg's law. If the extra distance travelled by the lower of two parallel incident X-rays is equal to an integer of the wavelength ($2d\sin\theta$), constructive interference occur and the reflected X-rays are in phase. B.) The 2D representation of Edwald's sphere. A set of crystal planes (hkl) are separated by a distance, d, and located at the origin O. The reciprocal lattice of the crystal (grey) is placed at the reciprocal lattice origin O*. The reciprocal vector O*P is normal to the specific set of hkl-planes and has the length of 1/d. AO* is equal to $2/\lambda$ and Bragg conditions are thus fulfilled for the reciprocal lattice point P. The reciprocal lattice is rotated along with the crystal during data collection, allowing more reciprocal lattice points, each representing a set of hkl planes, to cross the sphere.

When a reciprocal lattice point crosses Edwald's sphere, the Bragg conditions are met and diffraction occurs. A Bragg peak can hence be recorded on the detector. To sample all of the reciprocal lattice points of the crystal, all of them have to be brought into diffracting conditions. The crystal is therefore rotated within the X-ray beam when collecting data from a single

crystal. The ways by which the electron density within the unit cell later can be obtained from the recorded intensities, are further described in chapter 4.

## 3.2 X-ray Free-Electron Lasers (XFELs)

When a crystal is exposed to X-ray radiation, some of the photons will scatter elastically and the energy of the photon is conserved after the scattering event. On the contrary, some of the photons will be absorbed by the sample, causing free radicals to be released [67]. The events of ionising radiation are referred to as radiation damage. As a consequence of radiation damage, the diffraction quality of the crystal will be reduced during data collection and the chemical properties of the sample will eventually be altered. The most successful strategy to deal with the constraints caused by photon absorption events, has been to work at cryogenic temperatures. However, the field of serial femtosecond crystallography and the X-ray Free-electron Lasers (XFELs) have in the last years provided ways to overcome the issue of radiation damage.

In 2009, the first XFEL pulses were produced at the Linac Coherent Light Source (LCLS). In comparison to 3rd generation synchrotrons, XFELs produce shorter and more intense X-ray pulses. The peak brilliance of XFEL radiation is approximately ten orders of magnitude larger compared to X-ray radiation produced at synchrotrons [68]. The XFEL bunches are also much shorter, in the femtosecond range, which is three orders of magnitude shorter compared to a synchrotron. In contrast to the circular shaped synchrotron rings, XFELs are situated in kilometer-long linear tunnels. At XFELs, electron pulses are accelerated along a long linear accelerator (LINAC) and thereafter passed through a long array of switched dipole magnets, called the undulator. When the electrons travel through the undulator magnets they will be forced to oscillate and thereby emit radiation. The intense X-ray pulses contain about $10^{12}$ of photons, delivered with a pulse duration of tens of femtoseconds [67]. When a sample is placed into the focus of such an intense beam, it will be completely evaporated. However, full destruction on the sample will not occur until after the X-ray pulse has travelled through the sample, making it possible to collect diffraction data. This is because the femtosecond X-ray pulse is shorter than it takes for atoms to move, a principle referred to as diffraction before destruction [69, 70]. The

advances of XFEL sources has made it possible to determine the structure of protein crystals at biologically relevant temperatures with minimized consequences of radiation damage. Although, latter studies have indicated that the data collected from the high intensity X-ray pulses at XFELs may still suffer from radiation damage and that the effect is not fully understood [71].

## 3.3 Sample delivery at XFELs

The increased dose tolerance during data collection at XFELs has enabled diffraction from smaller crystals to be recorded. As the crystal is destroyed after a single X-ray pulse, new sample has to be delivered to the beam continuously. As a result, one crystal gives rise to a single diffraction pattern. In SFX, thousands of diffraction patterns from individual crystals have to be collected to generate a full data set covering all reflections of the crystal lattice. In SFX experiments, micro-crystals are used to avoid wasting sample and to correlate with the injection systems used at XFELs.

The first injection system to be developed was the gas dynamic virtual nozzle (GDVN), where the crystals are delivered to the beam in solution [72]. The nozzle is composed of two capillaries and the sample is pushed through the inner capillary by water from an HPLC pump. The size of the inner capillary usually varies from 50-100 $\mu$m and inlet filters are used to prevent larger crystals from clogging the nozzle. High pressured helium gas flows in the larger outer capillary to create a thin elongated jet of the sample. The minimal rate with which sample can be flown is around 10 $\mu$l/min, meaning that most of the sample will flow through the beam without being probed by X-rays. The GDVN injection system hence put high demands on the sample amount and several hundreds of milligrams to grams of protein can be needed for a single experiment. The high sample consumption called for development of new injection systems, where the sample flow-rate could be reduced. Several systems have been developed and among them are the fixed target injectors [73, 74] and the acoustic injectors for drop-on-demand principle [75, 76].

One commonly used system is the viscous injector, which initially was intended for microcrystals of membrane proteins grown in liquid cubic phase (LCP) [77]. This system is also driven by an HPLC pump and gas

is used to direct the flow. However, due to the high viscous carrier media the sample can be ejected from the nozzle at lower flow rates (> 0.3 $\mu$l/min) [77, 78]. Crystals which have not been grown in LCP originally can be mixed with viscous media [79, 80] preceding sample loading into the reservoir. An advantage with the viscous injection system, is as mentioned that it consumes less sample than the GDVN. On the other hand, the crystal solution has to be mixed with the grease matrix which can have affects on the crystal quality. Different grease matrices also give rise to different amounts of background scattering. It is crucial to find the right parameters for sample injection to work during the precious hours of SFX experiment. The best carrier media has to be discovered and the crystal size and density have to be optimized for the sample to flow smoothly.

## 3.4 Pump-probe experiments

Many of the fundamental reactions that occur in nature, and which are of great interest for investigation, involve molecular dynamics on femto-to millisecond time scales. The development of XFELs has combined the spacial resolution of X-rays (angstrom to sub-angstrom resolution) with a temporal resolution down to femtosecond time scales. XFELs have therefore dramatically improved the possibilities in the field of structural biology and the study of protein dynamics [81]. In SFX pump-probe experiments, the reaction of interest is initiated/triggered inside the protein crystal. The trigger can be a light pulse for light activated reactions [82, 83], or the addition of a substrate when studying enzymatic reactions [84]. The structural composition of the protein can thereafter be probed with X-rays at several different time delays. By capturing enough snapshots of the protein state at different time points during the reaction, a "molecular movie" of the structural changes can be constructed. A schematic illustration of the experimental set up during a pump-probe SFX experiment is shown in Fig. 3.2.

When performing light induced SFX experiments, the protein reaction inside the crystal is initiated using a pump laser prior to X-ray exposure. The pump laser generates light pulses of the specific wavelength necessary to trigger the reaction of interest. It is of importance that the laser spot is big enough to illuminate the whole crystal and intense enough to trigger a large portion of the chromophores within the single-photon regime, without

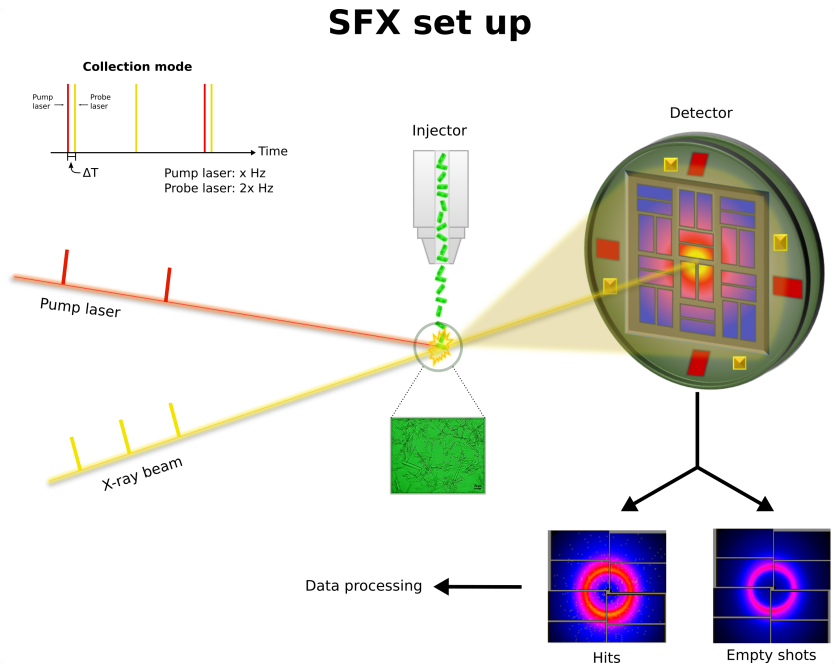


**Figure 3.2: Pump-probe SFX experimental set up**. Crystals are illuminated with light before they arrive at the interaction point with the XFEL pulses and give rise to diffraction patterns on the detector. Data collection during a pump-probe experiment can be collected in different modes depending on the repetition rate of the pump and probe lasers. The collection mode represented in the figure is alternating light-dark data collection. As the repetition rate of the probe laser is twice that of the pump laser, every second shot will be dark. Hits are sorted with Cheetah and further processed with CrystFEL.

damaging the crystal. Laser fluences that are too high can cause some chromophores to absorb multiple photons, resulting in signals corresponding to multi-photon absorption events.

After a predetermined time delay, the crystal will reach the X-ray beam and be probed by an X-ray pulse. Upon that, a diffraction pattern will be recorded on the detector before the crystal is destroyed. The time delay depends on the difference in timing between the pump and the probe laser, as well as the travelled path distance of the jet. Careful alignment of the laser pump and the X-rays are therefore extremely important for high time precision. Each X-ray laser shot arrives at a time difference ( $\pm$ 250 fs) compared to the nominal time ($t_0$), resulting in a relative arrival timing jitter of ~500 fs. A timing tool has to be implemented in order to accurately tag each shot with a relative time delay to $t_0$ [85–87]. The temporal resolution of the experiment is moreover limited by the pulse length of the pump laser (<100 fs), the pulse length of the X-ray probe (<50 fs) and the detector read-out rate. The detector has to be able to match the repetition rate of the X-ray probe (120 Hz at LCLS-I and 30 Hz at SACLA). The detectors used at LCLS-I and SACLA are the Cornell SLAC Pixel Array detector (CSPAD) [88] and the multi-port charge-coupled device (MPCCD) [89], respectively. A higher repetition rate of the probe laser also requires a faster sample flow to avoid light contamination from crystals being illuminated by a previous laser pulse.

A diffraction pattern, resulting from an X-ray pulse probing a microcrystal, containing enough Bragg spots is classified as a "hit" [90]. Occasionally, two or more crystals will be probed by the same X-ray pulse generating a multi-hit, or pass through the sample without interaction with any crystal, giving rise to an empty shot. The hit rate describes the percentage of X-ray pulses which are generating hits on the detector. The crystal density has to be optimized during an experiment to obtain a high hit rate without clogging the injection system. A large portion of the sample never gets probed by the X-rays and goes straight to the waste collector. Parameters such as injection system, flow-rate and crystal density are consequently essential in terms of efficient data collection.

## 3.5 Data collection of phytochromes at XFEL facilities

The resting state structure of the PAS-GAF fragment from *Dr*BphP, presented in **paper I**, was obtained from data collection performed at CXI at the Linac Coherent Light Source (LCLS) located in SLAC National Accelerator Laboratory, USA. X-rays (9.5 keV) were delivered with a repetition rate of 120 Hz. The GDVN nozzles were used for sample injection of the crystals carried in their mother liquid. Before loading the crystals into the reservoirs, they were concentrated and filtered through 20 $\mu$m filters. Prepared reservoirs were thereafter kept at 4° C until they were transferred and mounted inside the hutch. The average flow rate during data collection was 30 $\mu$l/min and the sample was injected to the beam using diverse nozzle sizes (50-100 $\mu$m in diameter). Due to clogging of nozzles and low crystal density, the hit rate during our experiment at LCLS was very low (only a few %) which resulted in slow data collection.

Remaining SFX experiments, which have generated results included in **paper I-IV**, were carried out at the SPring-8 Angstrom Compact free electron LAser (SACLA), Japan. The XFEL laser at SACLA was operated at 30 Hz, generating X-rays of 7 or 10 keV. The viscous injector was used for all of these experiments and the crystals were mixed with the high viscous media Superlube (Syncho chemical corp.). The crystals were concentrated and mixed with the grease matrix before being transferred into reservoirs. The sample flow used during these experiments spanned from values of 0.5-4.5 $\mu$l/min and the nozzle sizes varied between 50-125 $\mu$m.

Diffraction patterns of light activated crystals were recorded in some of these experiments; **paper II** includes time points of 1 ps and 10 ps, whereas **paper III** includes data collected at time delays spanning from $-1.8$ ps to 2.7 ps. Data collection varied from recording patterns in a mode of only dark, only light and dark/light interleaved. The wavelength of the pump laser was 640 nm and the photon fluences used were 1.7 mJ/mm$^2$ and 1.3 mJ/mm$^2$, in **paper II** and **paper III** respectively. A power titration of the pump laser was performed in **paper II**, spanning photon densities between 0.2-1.7 mJ/mm$^2$. A timing tool was furthermore implemented in this experiment to obtain accurate time precision.

# Chapter 4

# Analysis of X-ray crystallography and SFX data

Succeeding data acquisition, processing and refinement procedures have to be performed in order to obtain structural information. The methods and strategies that were used to analyze the data collected on phytochromes are outlined below.

## 4.1 Data processing and refinement

A synchrotron X-ray crystallography experiment will generate a set of diffraction patterns containing multiple Bragg reflections ($hkl$). The structure factor of a reflection ($hkl$) is described by the structure factor equation (see 4.1). $f_j$ is the atomic structure factor and $x, y, z$ are the atomic positions within the unit cell. The structure factor ($F_{hkl}$) represents the wave that caused the reflection ($hkl$) and has an amplitude, $|F_{hkl}|$, and a phase, $\phi_{hkl}$. The electron density ($\rho$) at a certain position ($x, y, z$) in the unit cell (with a volume $V$) can be calculated by the Fourier transform of the structure factors (see 4.2).

$$F_{hkl} = \sum_{j=1}^{n} f_j e^{2\pi i} \left(hx_j + ky_j + lz_j\right) \tag{4.1}$$

$$\rho(x, y, z) = \frac{1}{V} \sum_{h} \sum_{k} \sum_{l} |F_{hkl}| \, e^{-2\pi i(hx+ky+lz)+i\phi_{hkl}} \tag{4.2}$$

Both the structure factor amplitudes and the phases are hence required to calculate the electron density. The structure factor amplitudes can be obtained from the measured intensities of the reflections. The phase information, however, is lost during the experiment which gives rise to the so called phase problem. One strategy to overcome the phase problem is molecular replacement (MR). The approach in MR is to borrow initial phases from a homologous model which is structurally similar to the protein of interest. The phases are then further refined to better fit the experimental data during the refinement process.

Processing of diffraction data from X-ray crystallography experiments proceeds through several steps. *Determination of the unit cell parameters and the space group* is achieved from a few diffraction patterns. The obtained information is then used for *indexing and integration* of the whole data set. Crystallographic software such as MOSFLM [91,92] and XDS [93] have been developed for these purposes. The data is furthermore *scaled and merged*, generating a single file containing the structure factor amplitudes for all the Bragg reflections. Molecular replacement or some other phasing method such as multiple isomorphous replacement (MIR) or single-wavelength anomalous diffraction (SAD), can be used to *obtain the phases*. The succeeding step is to *calculate the electron density* through a Fourier transform and subsequently build an *initial model* into the electron density map. The initial model will provide new phases that are used to calculate an improved electron density map, which is used for a new round of model building. Several iterations of these steps are performed for further *refinement* of the structural model. The refinement process can be validated by determination of the $R_{work}$ (see 4.3), which describes the agreement between the calculated structure factors from the model and the observed structure factors from the experimental data.

$$R_{work} = \frac{\sum ||F_{obs}| - |F_{calc}||}{\sum |F_{obs}|} \tag{4.3}$$

To avoid overfitting of the model during refinement, cross-validation is introduced by the $R_{free}$ value. A small subset of the reflections, usually 5-10 %, is excluded from the refinement process and used to generate $R_{free}$. $R_{work}$ is generally ~2 % lower than $R_{free}$ and a decrease in $R_{work}$ without improvement of $R_{free}$ is an indication of overfitting [62]. The model

should furthermore be validated from a chemical point of view to make sure that bond lengths, bond angles and torsion angles etc. all falls within the expected values [94]. Crystallographic software packages such as CCP4i2 [95] and Phenix [96] contain the programs needed for data processing and refinement.

As stated earlier, the data acquisition in conventional X-ray crystallography and SFX experiments differ in many aspects. New software such as Cheetah [90] and CrystFEL [97] have been developed for SFX data to support the increased demands on fast data reduction and processing, respectively. As a result of sample injection by jetting, each reflection will be measured several times and a full SFX data set can contain several thousand of diffraction patterns. Each diffraction snapshot is a representation of a slice through reciprocal space, at a random direction, and the reflections recorded are often partial. All diffraction snapshots come from individual crystals, which may vary slightly in size, shape and quality. Furthermore, the X-ray beam fluctuates between shots which introduces additional variation. Therefore, the redundancy/multiplicity required in these type of experiments must be high to meet the challenges of variation and to integrate and merge all patterns into a cohesive data set [98]. Some figure of merits important to validate SFX data is CC1/2 and $R_{Split}$, which are based on the consistency within the data set. CC1/2 is the Pearson correlation coefficient of the two partial data sets after splitting the entire data set in half. $R_{Split}$ also results from dividing the entire data set in two parts and merging them separately before comparison of the two intensity lists [99].

## 4.2 Difference electron density maps

The purpose of time-resolved crystallography is to capture structural states of the protein at different times after a reaction has been initiated. For light induced reactions, difference maps ($F_{obs} - F_{obs}$) can be calculated to compare the dark and light diffraction data from the experiment. Difference structure factor amplitudes are computed as follows: $|\Delta F_{obs}| = |F_{obs}^{light}| - |F_{obs}^{dark}|$. As no phase information is recorded, the phases have to be obtained from a refined dark structure. Before subtracting the data sets from one and another they should be scaled against each other, to ensure that the differences are caused by light induced structural changes and not

to an off set between the two data sets. The structure factor amplitudes can be scaled to each other by first scaling $|F_{obs}^{dark}|$ to the refined model $|F_{calc}^{dark}|$, and thereafter $|F_{obs}^{light}|$ to $|F_{obs}^{dark}|$. Weighted difference maps can be obtained by applying the Bayesian weight ($w$) to the difference structure factor amplitudes. The intention of weighted difference electron density maps is to reduce the impact of outliers and to improve signal to noise [100, 101]. The difference electron density map, $\Delta\rho$, indicates where electron density has disappeared from the dark state (negative) and appeared in the light state (positive). The difference features present in the map, above the noise level (roughly 3 $\sigma$), can be interpreted as structural changes between the two states. Initial difference maps are calculated during the actual experiment to look for signal and guarantee that enough data has been collected for a certain time point. The difference electron density maps are improved later on when the dark state phases have been properly refined.

## 4.3 Representations of difference electron density

The purpose of SFX experiments is typically to follow structural changes over time and hence several data sets at different times during the studied reaction have to be collected. There are several ways to present changes that occur in a sequence of difference electron density maps. The minimum/maximum value of the electron density for specific features can be read out manually from each map using the graphic software COOT [102]. However, as is always the case in manual investigation, this approach bares the risk of imposing bias. Which features in the map that are to be considered meaningful in terms of signal depend on the investigator to a large extent. Furthermore, this kind of representation carries the disadvantage of not presenting an overview of the data. Lastly, it is tedious work to extract the difference electron density values for several features in several maps.

Wickstrand et al. [103] developed another approach to the task of presenting difference electron density data, using a more objective way of displaying the changes. They converted the representation of three-dimensional difference electron density maps into one-dimensional plots. This is done by defining a sphere, set to a certain radius, around each atom in the resting state model. For a certain map, the positive and negative electron density amplitudes within each sphere are extracted and averaged separately. This

process yields one positive and negative amplitude value for each atom in the protein. The amplitude functions (one +/- value for each atom) can then be plotted as a graph following the trace of atoms over the whole protein chain or for selected residues (see Fig. 4.1). By plotting several maps together, the structural changes in the protein can be followed over time.

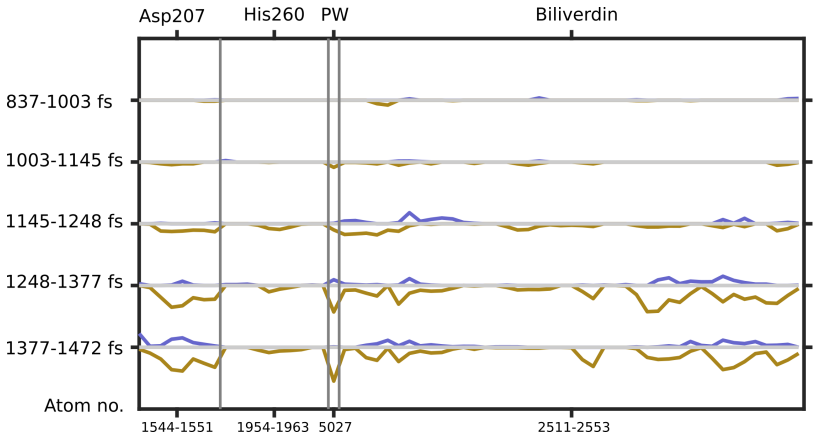


**Figure 4.1: One-dimensional representations of difference electron density maps.** The mean positive (blue) and mean negative (yellow) amplitudes plotted for certain atoms within the chromophore binding pocket in subunit A (plotted along the X-axis). The electron density amplitudes was extracted from a sphere set to 2 Å around each atom with a 3 $\sigma$ cut off as a threshold.

The parameters that need to be set by the investigator are the radius of the sphere (i.e. 2 Å), the threshold of the lower electron density cut off (i.e. $\pm$ 3 $\sigma$) and the grid spacing used when extracting the amplitude values (i.e 0.5 Å). With this approach, all the difference electron density around the atoms will be taken into account rather than specific features which have been determined manually. An overview of the data, as well as the timing and location of the changes, are illustrated by this presentation. Therefore, this approach becomes very useful as an initial step when analysing a set of difference electron density maps. On the other hand, the representation of these maps as one-dimensional plots does not give any information about the direction or extent of the structural changes.

Hence, figures showing the position of the difference electron density features in space are still required to understand how the structure is moving

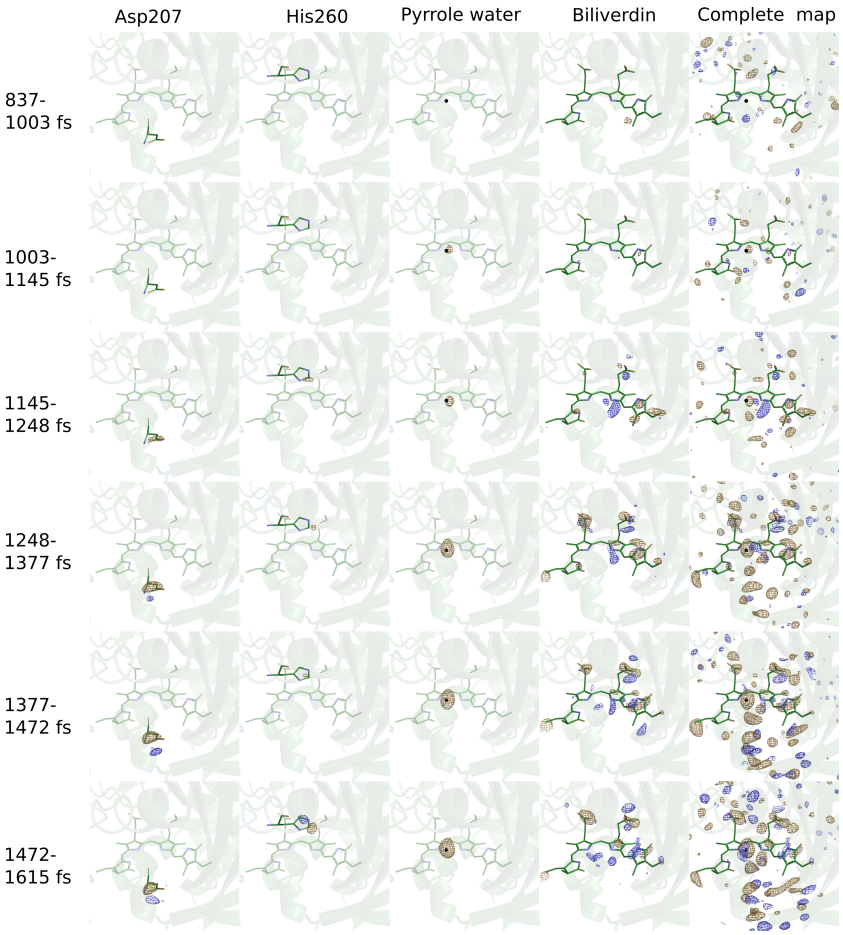


**Figure 4.2: Difference electron density maps**. Positive (blue) and negative (gold) difference electron density displayed for certain parts of the chromophore binding pocket. A selection of maps ranging from 837 fs to 1472 fs have been chosen to illustrate how signal evolution occurs over time. Difference electron density maps are contoured at 3.5 $\sigma$.

(see Fig. 4.2). In summary, one-dimensional graphs and figures of the three-dimensional difference electron density maps, work exceptionally well as complementary representations of the changes in difference electron density over time.

## 4.4 Refinement of light activated structures

When difference electron density maps have been calculated, they can be used to refine structures of light activated states of the protein at different time-delays. However, refinement of light structures are tricky as the light data at a certain time delay results from a mixture of light and dark structures. The population of proteins in the crystals that correspond to a certain light induced state is often low, depending on the quantum yield of a specific photoreaction. As in the case of phytochromes, the population of excited proteins which proceed to Lumi-R correspond to ~10-15% [5, 19, 20, 104, 105]. As a result the observed difference map is heavily biased to the dark state. Furthermore, a difference map only reports on the structural changes whereas the goal is to obtain an absolute structure of the light state. There are several approaches to go about refinement of light structures. One strategy is to add alternative conformations to the structure according to the light occupancy and let these refine against the light data (Paper VII). Another approach is to calculate extrapolated structure factor amplitudes, $|F_e|$, where the measured difference structure factor amplitudes are extrapolated, generating the pure structure factor amplitudes of the light induced state: $|F_e| = |F_{calc}^{dark}| + \alpha * |\Delta F_{obs}|$. $\alpha$ is inversely related to the population in the photoinduced state (*P*) as: *P*=100/$\alpha$ x 2 (in percent) [106]. Phases are borrowed from the dark state model to calculate an extrapolated electron density map. The dark state model is then placed into the extrapolated map and manually refined into a light model using real space refinement in COOT [106, 107].

The refined structural models, dark and light structures, can be used to obtain a calculated difference electron density map. If the structures representing the dark and light protein states are truly representing the experimental data, the observed and the calculated difference electron density ($\Delta\rho_{obs}$, $\Delta\rho_{calc}$) should be highly similar for a certain time point. Hence comparison of the two maps to each other, by visual inspection (see Fig.4.3) or by calculating a difference difference map ($\Delta\rho_{obs} - \Delta\rho_{calc}$), will indicate whether the structures have been rightfully modelled. The correlation between $\Delta\rho_{obs}$ and $\Delta\rho_{calc}$ can furthermore be evaluated by calculating Pearson Correlation Coefficient (PCC). PCC values can beneficially be used to guide the refinement of certain regions of the protein structure.

Real space refinement of the light structure proceed until the agreement

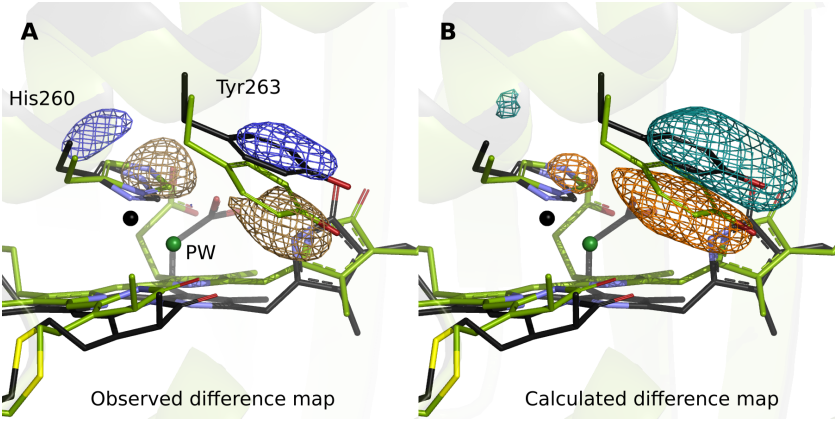


**Figure 4.3: Comparison of observed and calculated difference electron density maps**. A.) The $\Delta\rho_{obs}$ displayed around $His_{260}$ and $Tyr_{263}$. B.) The same view displayed with the $\Delta\rho_{calc}$. The electron density is displayed at 3.3 $\sigma$ and 3.5 $\sigma$ for the observed and calculated map, respectively. The difference peaks present in the observed difference map are reproduced in the calculated map.

between the observed and calculated maps reach satisfying levels. The refined dark and light models are further used to calculate difference phases which can be combined with the observed difference structure factor amplitudes to calculate phased extrapolated structure factors. Final refinement of the light model is then performed in reciprocal space using the phased extrapolated structure factor amplitudes [106, 107].

# Chapter 5

# The initial photoresponse in Phytochromes

The time-resolved X-ray crystallography experiments conducted in **papers II-III** generated important information of the primary photoresponse in phytochromes. The major findings from these papers will be presented in chapter 5.

## 5.1 A collective photoresponse for the chromophore binding pocket

**Paper II** presents serial femtosecond X-ray crystallographic data of the PAS-GAF fragment from *Dr*BphP, captured at 1 ps and 10 ps after red-light (640 nm) illumination. The observed difference electron density maps indicate that a collective photoresponse of the chromophore and the surrounding binding pocket has occurred already at 1 ps after photoactivation. The structural changes include a liberation of the chromophore from its anchoring protein residues. The broken interactions are either caused by or lead to rearrangement of the biliverdin propionate groups and two protein regions, referred to as the capping helix (residues 275-269) and DIP region (residues 201-209). Both of these residue stretches move away from the chromophore, resulting in an expansion of the binding pocket (see Fig. 5.1 A). The capping helix and DIP region include several amino acids which are highly conserved among phytochromes. The side-chain movements of $Ile_{208}$, $Asp_{207}$, $Tyr_{176}$, $His_{260}$ and $Tyr_{263}$, all participate in introducing a less restrained environment around biliverdin (see Fig. 5.1 B). Moreover, $Asp_{207}$

and $Tyr_{263}$ go through a scissor-like movement, resulting in a separation of the two residues (see Fig. 5.2 A). The structural rearrangement discovered for these amino acids indicate that the signal may have reached the tongue region as early as 1 ps after photoabsorption. However, a protein construct including the PHY-domain must be investigated for this speculation to be confirmed.

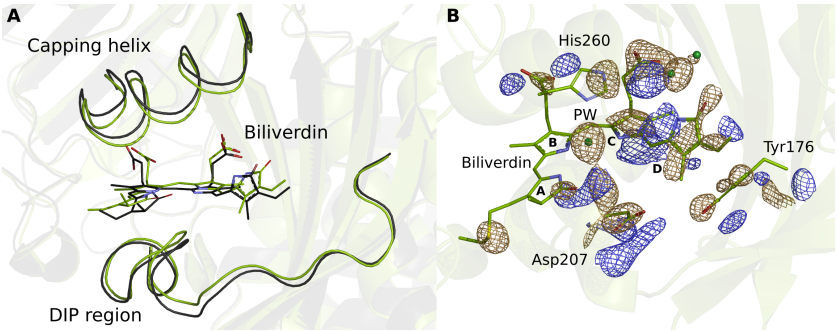


**Figure 5.1: Expansion of the chromophore binding pocket**. A.) The dark state structure (green) and 1 ps structure (black) illustrate that the chromophore binding pocket have expanded upon light activation. B.) The observed difference electron density map at 1 ps displayed for parts of the chromophore binding pocket. Positive (blue) and negative (yellow) difference electron density is contoured at 3.3 $\sigma$.

The observed changes in the local environment of the chromophore are accompanied by structural changes of biliverdin itself. A majority of the chromophore atoms, including the A-,C- and D-ring atoms and the two propionate groups, indicated strong negative difference electron density (see Fig. 5.1 B). Isomerization of the D-ring is thought to be the initial trigger for photoactivation in phytochromes. We modelled the D-ring rotation in various angles and calculated difference maps and Pearson correlation coefficient (PCC) values from each conformation. The PCC values were based on the comparison between the observed and calculated difference electron density within a sphere of 2 Å around the D-ring. The calculated map with the best agreement to the observed difference maps was obtained when the D-ring was modelled in a twisted conformation as demonstrated in Fig. 5.2 B.

Furthermore, several water networks connecting the chromophore and protein were found to have rearranged. Among them where the conserved

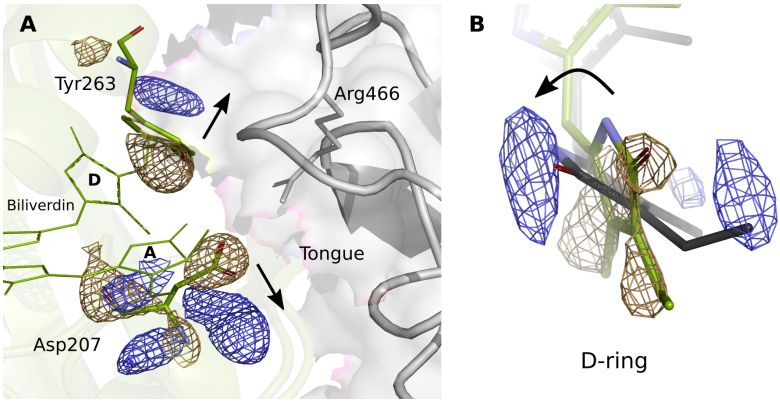


**Figure 5.2: Structural changes of chromophore and conserved amino acids** A.) The difference electron density features around $Asp_{207}$ and $Tyr_{263}$ indicate that the residues separate from each other in a scissor-like movement. $Asp_{207}$ is bonded to $Arg_{466}$, located in the tongue region, in the Pr-state when the PHY domain is present (pdb code: 4q0j, grey). Panel A illustrates the movements of the aspartate and tyrosine residues and how they are located in respect to the tongue region within the protein. B.) The dark (green) and 1 ps (black) structures displayed for the D-ring together with the observed difference map. The positive (blue) and negative (gold) electron density features, contoured at 3.3 $\sigma$, imply that the D-ring twists around the C15=C16 bond.

waters located in the D-ring cavity, which connect the chromophore, $His_{290}$ and $Ser_{272}$ in the Pr dark state. Surprisingly, the pyrrole water was dislocated from its original position in the middle of the chromophore (see Fig. 5.1 B). This water is present at the same position in all Pr and Pfr structures solved so far. The location to where the pyrrole water moves is not unequivocal from the difference maps. Nevertheless, our results illustrate that the water does not stay in the same position throughout the photocycle.

Taken together, a highly collective response is observed at an early stage in the phytochrome photocycle, where the D-ring is in a twisted position. These findings were confirmed in two separate experiments, indicating that the results are highly reproducible.

## 5.2 Two separate delay stages of structural rearrangement in the early photoresponse

The aim of **paper III** was to investigate how the structural changes observed at 1 ps in **paper II** arose. Accordingly, data were collected at time-delays spanning from -1812 to 2727 fs. The new difference electron density maps revealed that the collective response of the chromophore and the surrounding binding pocket observed in our previous paper, does not evolve instantly upon photoabsorption. Instead these changes grow above the noise level at delayed time points (~1.0 ps) and the signal continues to increase in strength throughout the complete data set (up to 2.7 ps) (see Fig. 5.3). As already mentioned, highly similar structural changes were observed in both of our experiments at SACLA. Several positive and negative features were identified at the same positions in both difference electron density maps. The reproducible results and directed structural changes make it tempting to assume that the response observed in our data is part of a signalling mechanism used by phytochromes. However, it is difficult to foresee the effects that factors such as pH, crystal packing, excitation wavelength and photon fluence have on the molecular mechanism caused by photon excitation.

Except for the collective response observed at later time points, the new data generated information about the initial structural changes upon light activation. Two conserved tyrosine residues, $Tyr_{176}$ and $Tyr_{263}$, were found to be the first amino acids to move upon photon excitation. These structural changes were found to exceed the noise level already within a few hundred femtoseconds (see Fig. 5.3). These two residues are highly conserved among phytochromes and are important for proper photoconversion [32, 108–110]. It can be speculated that these residues move as a result of relaxation processes of the excited state or that they take part in electron transfer events. However, more data around time zero need to be collected to fully investigate the role of these tyrosine residues in the early signal transduction.

It can be concluded from our experiments that the state we observe in our SFX data has gone through extended structural rearrangement in comparison to the Pr structure. Large structural changes in the chromophore and the surrounding binding pocket already at 1 ps are not in agreement with the proposed model for photoactivation in phytochromes [110, 111]. In this model the system stays on a similar energy potential surface before and after

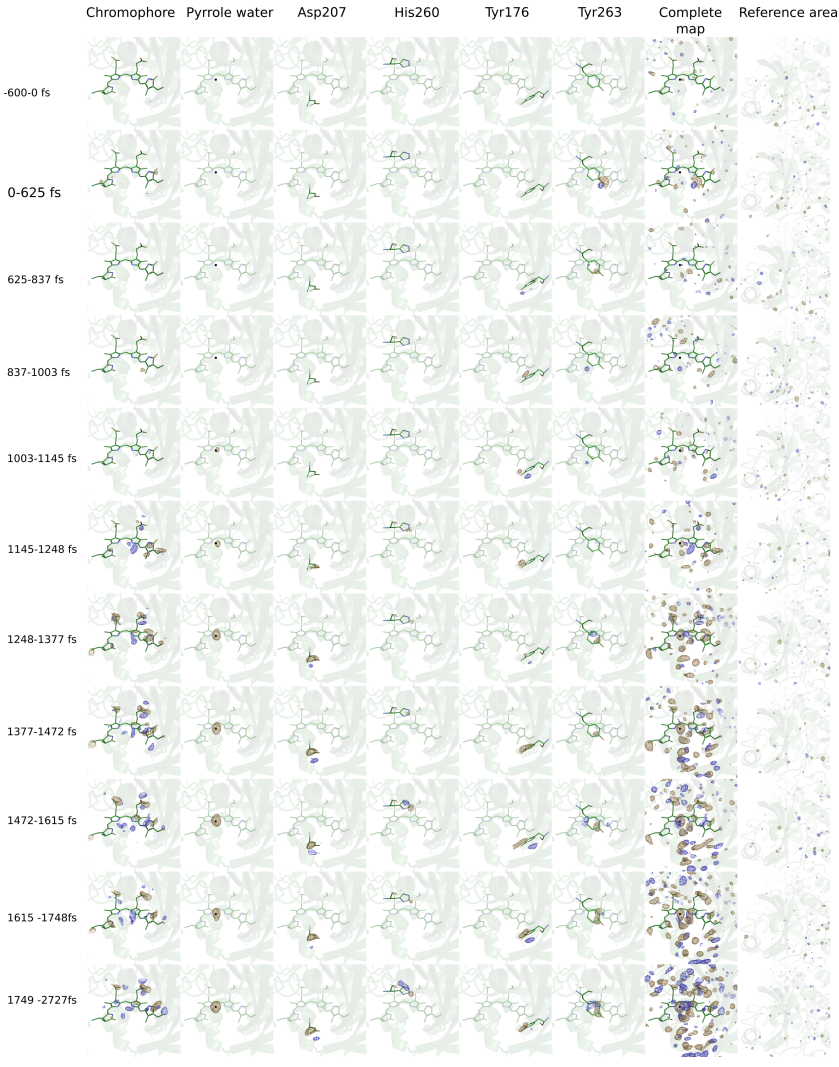


**Figure 5.3: Evolution of structural changes upon excitation in *Dr*BphP.** The difference electron density displayed for the chromophore and selected residues. The second last column (to the right) displays the complete map for the chromophore binding pocket. The last column displays the complete map for a reference area in the outer part of the protein. The difference maps are contoured at 3.5 $\sigma$ and positive and negative densities are colored blue and gold, respectively.

the D-ring twist. In **paper III** we therefore propose a new model for photoactivation in *Dr*BphP, in which our SFX structure with the twisted D-ring represent a new state (X). This state is lower in energy than the excited state ($S_1$) and form on a short picosecond time scale ($\sim$1-2.7 ps). Data at succeeding time points need to be recorded to follow the evolution and life time of state X. Furthermore, complementary spectroscopy measurements should be performed on the same protein fragment to extend the investigations of our proposed state X. Such measurements can also bring more clarity to how different experimental settings affect the molecular mechanism that results from photon excitation.

# Chapter 6

# Single particle Cryo-EM

An important key to understand the mechanism that phytochromes use to photoconvert lies in solving a full-length structure, including the output domains, to atomic resolution. No conditions have yet been found which yield well-diffracting crystals for X-ray crystallography experiments. On these grounds, a project was started with the aim to solve a full-length *Dr*BphP structure to near-atomic resolution using single particle cryo-EM. A description of the initial stages of the project is included in this chapter in order to document the preliminary results. The method has a lot of potential for structural studies on phytochromes and the project is still ongoing.

## 6.1 Introduction to single particle cryo-EM

X-ray crystallography is a powerful technique and the majority of structures deposited in the protein data bank (PDB) were determined by this method [112, 113]. However, not all proteins are prone to crystallize. Large complexes and highly flexible proteins are especially difficult targets in protein crystallization. Fortunately, major progress has been made in the field of single particle cryogenic electron microscopy (cryo-EM) over the past years. The advances have provided an alternative method to solve protein structures down to atomic resolution without the need of crystals.

In single particle cryo-EM, proteins are frozen in solution on grids and viewed under an electron microscope. The use of an electron beam, rather than a beam of photons in the visible region, provides the possibility to study the objects to higher resolution. Light microscopes (using visible light, 390-760 nm) are limited to resolve objects of 200 nm, whereas electrons have

shorter wavelengths and allow for three orders of magnitude higher resolution [114]. Irradiation of the protein sample with electrons give rise to 2D projection images that are recorded on a detector. 2D projections of an object from several different directions can later be combined to reconstruct a 3D model of the macromolecule [115, 116]. Before the proteins can be viewed in the microscope they are flash frozen in a buffer solution on a metal mesh support grid (3 mm in diameter) [117]. The grids are covered with a layer of carbon holey film and the proteins are frozen across the holes in a thin layer of vitreous ice. Although freezing will make the protein sample more tolerant to radiation, low electron doses are still required to avoid sample damage. As a consequence, the recorded images have very poor signal to noise ratio (SNR). A large number of 2D images are therefore required to average out noise and to obtain several different views of the studied protein [118]. The prediction that single particle cryo-EM theoretically could reach atomic resolution, was made many years ago [119]. Several technical breakthroughs such as development of direct electron detector cameras and computational algorithms have since then contributed to make these predictions reality [118, 120].

The resolution to which a structure of a macromolecule can be solved with single particle cryo-EM depend on many individual aspects. Factors such as the homogeneity of the sample, the contrast of individual particles, the number of views that are identified and the number of particles possessing these views, are all of importance. A project therefore normally starts with negative staining to characterise the sample properties before applying the aspect of vitrification. The sample should preferably have low degree of conformational and compositional variation, no aggregations and be equally distributed over the grid. First as satisfying grids or possibly 2D class averages are obtained by negative staining, the sample is ready for further investigation with cryo-EM. The process of generating satisfying cryo-grids involves further optimisation of buffer conditions, protein concentration, grid type and blotting time etc. to obtain a homogeneous sample in optimal ice-thickness. When promising cryo-grid conditions are discovered, the project can proceed with data collection and further structure refinement. The theory and practical aspects regarding data collection and subsequent steps in obtaining a structure are out of the scope of this thesis. Focus will instead be spent on the parts regarding sample and grid preparation, which eventually

led the project up to the point of data collection.

## 6.2 Sample preparation

As pointed out above, a well-behaving and homogeneous sample is crucial for grid preparation. Sample heterogeneity can arise from conformational or compositional variation within the protein sample. The compositional heterogeneity can be reduced to some extent through protein purification producers. A size-exclusion chromatography profile and analysis with SDS-PAGE provide information about the protein stability, the quaternary structure and the purity in regards to other macromolecules. Evaluation of the sample properties using these methods are therefore useful steps in the process of obtaining successful grids.

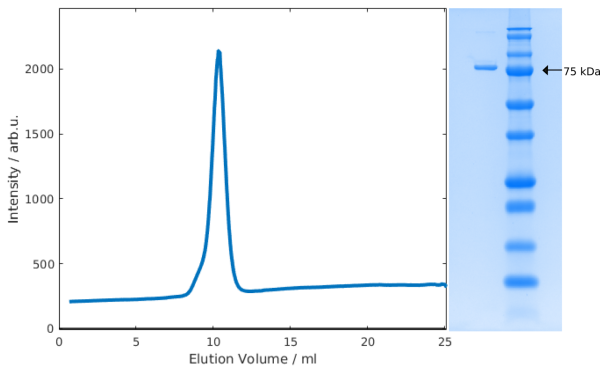


**Figure 6.1: Evaluation of protein purity and stability.** A small fraction of purified full-length protein, performed with nickel affinity and size-exclusion, was loaded onto a Superdex 200 10/300 GL column (24 ml bed volume). The sample eluted as a single peak with the centred fraction (containing 1.5 mL sample) having a concentration of ~1 mg/ml. Sample from this fraction was further analysed with SDS-PAGE. A single strong band could be observed at the expected weight of 86 kDa and a faint band was present between the 150 and 250 kDa bands of the ladder, most likely corresponding to the dimer.

The full-length phytochrome from *Deinococcus radiodurans* is a 172 kDa homodimer, classified as a rather small protein in the field of cryo-EM. The full-length protein was purified following the same strategy as described

in Chapter 2. Depending on the stability of the sample and the conditions during storage, the proteins can begin to aggregate over time. Therefore a common approach when studying proteins with EM is to run the sample through a gel filtration column right before grid preparation. The amount of sample needed for negative staining (a few $\mu$l of ~0.05 mg/ml) and single particle cryo-EM (a few $\mu$l of ~1 mg/ml) is less than for crystallography (several $\mu$l of ~5-30 mg/ml) [121]. An additional purification step was therefore performed on a fraction of the sample, using a smaller gel filtration column (Superdex 200 10/300 GL column). The size exclusion buffer used for purification of the full-length construct (30 mM Tris, pH 8) was a promising starting point for grid preparation, as less content of salt and organic molecules is beneficial in Cryo-EM for particle contrast [122]. A monodisperse peak in the chromatogram and a single band at the expected molecular weight on the SDS-PAGE gel, indicated a highly pure sample (see Fig. 6.1). The functionality of the protein was confirmed using UV-visible spectroscopy. As the results indicated a pure and functional protein sample the project proceeded with negative staining.

## 6.3 Negative staining

A pure sample in biochemical terms will not ensure that the particles appear homogeneous on the EM grid, as conformational flexibility can be present. To evaluate the homogeneity of the sample it has to be studied on the grid inside of the microscope. An electron microscope is maintained under vacuum to avoid scattering events of electrons as the beam travels from the source to the sample position. The vacuum would rapidly dehydrate a biological specimen, causing a structural collapse. The sample is therefore fixated and dehydrated on the grid prior to placement in the microscope [123]. There are several methods used for sample fixation, including staining of the macromolecules with heavy atoms [124]. In negative staining, the sample is coated in a layer of dried heavy metal solution, usually uranyl acetate for proteins. The high imaging contrast in negative staining electron microscopy comes from the particle of interest being less electron dense than the surrounding stain. The macromolecules appear as light objects in the image as they scatter little of the electron beam, whereas the surrounding electron dense stain scatter more of the electron beam and appear darker. As the sample is coated

with heavy atom the resolution is limited (approximately 18-20 Å) by the grain size of the stain [125]. The advantage of the high contrast between particles and background can be used for effectively evaluating the purity, heterogeneity and concentration of the sample. The short time needed for grid preparation makes the method a valuable tool for fast acquisition of low resolution information of the sample of interest.

The preparation of grids for negative staining is fast and starts with glow discharging of the EM grids. The procedure will make the grid surface negatively charged and hydrophilic, which facilitates an even spread of the buffer solution on the grid. The precise protocol for negative staining is rather individual in terms of incubation times and washing steps but the basics are highly similar. After the grids are hydrophilized, they are incubated with protein solution followed by staining with heavy metal solution. Excess liquid is blotted away on filter paper in between steps and after the staining procedure the grids are left to dry at room temperature. The full-length construct was prepared for negative staining electron microscopy using 200 mesh copper grids. The protein sample was diluted to a concentration of ~0.04 mg/ml and the grids were incubated with protein solution for approximately two minutes. The particles were stained for 15 seconds x2 using 2% uranyl acetate (in $H_2O$). The grids were dried in room temperature over night before they were visualized in a FEI Tecnai T12 120 kV microscope. The expected dimensions of the full-length BphP is approximately 80-90 Å wide and 140-180 Å long [44, 46]. Single particles of roughly these dimensions are seen across the grid in a variation of different views. Before enough data was collected to generate 2D class averages, the cryo-EM project was denoted time on the Talos Arctica microscope at the SciLifeLab in Stockholm for cryo-grid screening.

## 6.4 Cryo-grid preparation

The negative staining procedure bears, aside for resolution limitations, the disadvantage of dehydrating the sample and thus removing the proteins from their native state. Sample immobilisation caused by fast freezing maintains the aqueous environment around the proteins and simultaneously brings the advantage of making the sample more sustainable to radiation damage. The freezing has to be very fast (~$10^6$ °C/s) to prevent formation of crystalline

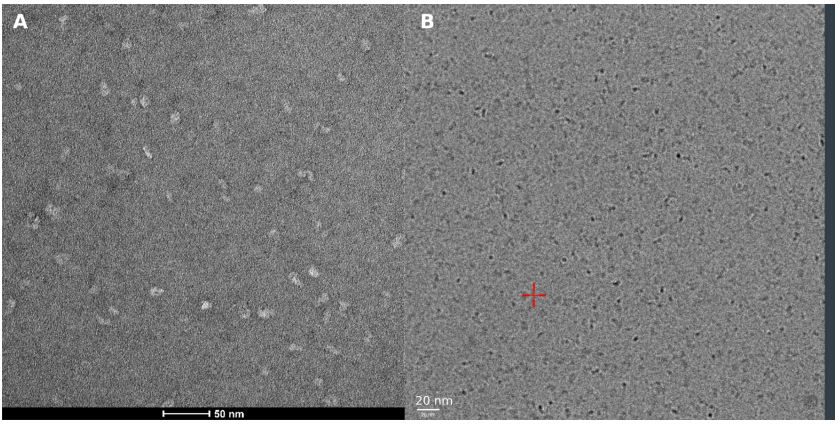


**Figure 6.2: EM images of the full-length *Dr*BphP** A.) Negative staining image of the full-length *Dr*BphP, stained with uranyl acetate. B.) A micrograph of the same protein fragment frozen on an EM gird.

ice [126]. Ice crystals affect the image quality as they diffract electrons and can also have an impact on the sample quality itself since ice formation withdraws water molecules from the sample. An automatic plunge freezer, i.e. a vitrobot, is used to achieve fast freezing and capture the particles in a thin layer of vitreous ice [127]. In this procedure a few microliters of the sample is placed on a grid and excess solution is blotted away on filter papers before the grid is plunged into liquid ethane (maintained around -180 C°). The use of ethane as a cryogen is preferred over liquid nitrogen because of its thermal conductivity, which is hundreds of times higher and allows for faster freezing. Liquid nitrogen is still used to cool down the cup in which ethane is liquefied and keep it cold during the plunge freezing process [127]. The ice should be as thin as possible (<100 nm) to maximise particle contrast and avoid multiple scattering events, but must be thick enough to cover the whole particles (usually 10-30 nm) [128]. The ice thickness often varies across the hole, being thicker at the edges and thinner in the middle and areas of good ice have to be selected for data collection. The proteins are ultimately frozen in their native state and captured in multiple random orientations. Unfortunately, a common problem is that particles freeze in a preferred orientation. One cause of this phenomenon rises from the fact that proteins tend to move towards the two air-water interfaces. As this process

occurs faster than the procedure of plunge freezing the grid, a majority of particles end up frozen in a preferred orientation at the top and bottom of the grid [117, 129]. Preferred specimen orientation will result in a low number of 2D class averages, preventing a 3D model from being reconstructed.

It is not always trivial to optimise buffer conditions, since a composition which promotes protein stability and functionality is not necessarily the best choice for freezing purposes. Solving a protein structure to atomic resolution using single particle cryo-EM is far from a straightforward procedure. Many rounds of returning to laboratory work and grid optimisation can therefore be required after the project has reached the point of data collection and structure determination.

Copper grids were initially used for cryo-grid screening of the full-length *Dr*BphP. Protein solution with concentrations varying from 0.5 to 1 mg/ml was frozen using the vitrobot at SciLifeLab in Stockholm. 3 $\mu$l of sample was applied to the grid and illuminated for 60 seconds either with red (665 nm) or far-red (785 nm) light. The grid was blotted against filter paper for 2 seconds, followed by an incubation time of 5 seconds before it was plunged in ethane and transferred to liquid nitrogen. The grids were stored in liquid nitrogen until visualized in the Talos Arctica microscope. An image of one of the first frozen grids containing the full length phytochrome construct is shown in Fig. 6.2.

## 6.5 Outlook of the project

The project has proceeded further and is currently in the iterative process of grid preparation, data collection, data processing and structure refinement. Initial electron density maps have been obtained of the full-length protein to a resolution of approximately 7.5 Å (see Fig. 6.3). A current hurdle is that the particles freeze in a preferred orientation and more data have to be acquired to resolve a larger part of the protein and to increase resolution. Hopefully the project will proceed to completion and reveal the coveted structure of the full-length *Dr*BphP at atomic resolution.

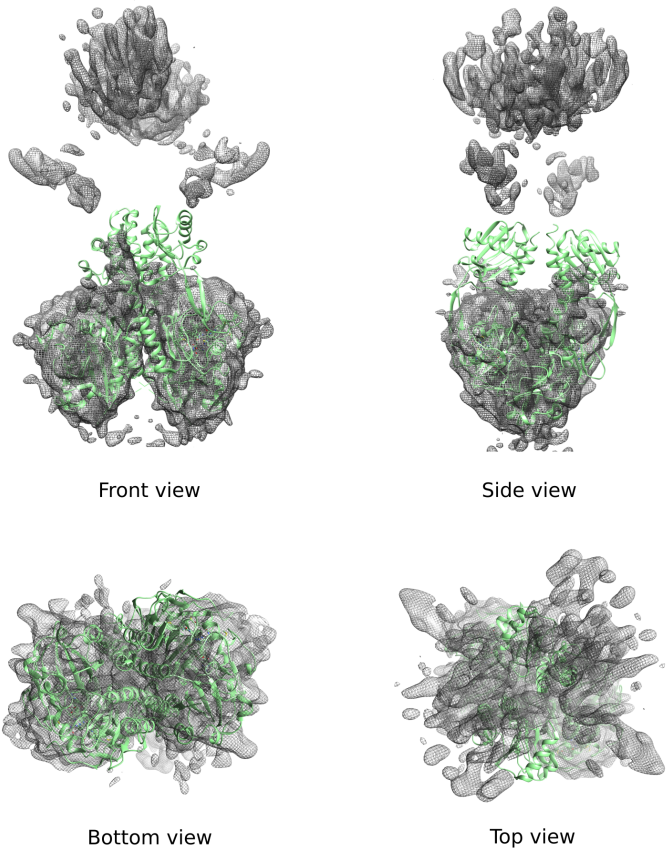


**Figure 6.3: 3D reconstruction of the full-length *Dr*BphP.** Homogenous 3D refinement of the full-length DrBphP using cryoSPARC. The 3D map is displayed from several different views together with a crystallographic model of PAS-GAF-PHY in the Pr-state (pdb:4O0P).

# Chapter 7

# Concluding remarks and future perspectives

## 7.1 Phytochrome photocycle

The work included in this thesis has been successful in growing microcrystals of the PAS-GAF fragment from *Dr*BphP. The crystals were used for SFX experiments to study the primary photoresponses of phytochromes. Data have been collected at several time points (spanning between 0-10 ps) to investigate the structural changes that occur after the chromophore is photoexcited. The results indicate that phytochromes utilize a highly collective mechanism where the chromophore and several waters and residues in the binding pocket cooperate in an early photoresponse. The data further reveal that two conserved tyrosine residues located in the D-ring cavity of the protein are the first residues to move as a result of photon absorption. Additional data have to be acquired at 0-1 ps to understand the details of how the signal is transferred from the chromophore to the surrounding binding pocket. Data acquisition at later time points (tens to hundreds of picoseconds), is also necessary in order to follow the evolution of the primary changes. The structural changes observed in the PAS-GAF fragment should furthermore be compared with those of the complete photosensory module (PAS-GAF-PHY). Crystals of the latter are therefore required to investigate how the signal is transmitted through the protein towards the output domains. We have solved the dark state room temperature crystal structure of the PAS-GAF-PHY fragment from *Sa*BphP (Paper IV). Hence the former difficulties in obtaining high-resolution diffracting crystals of the full photosensory core no longer prevent investigation of later steps in the photocycle. Further, the

structural changes have to be correlated with the findings across other fields and methods to be brought into a wider perspective of the photoactivation mechanism in phytochromes.

## 7.2 A full-length phytochrome structure

In order to study the full path of signal transduction, the investigations have to be aimed at the complete protein including the histidine kinase domains. A structure of the full-length protein to atomic resolution constitutes an essential step in this matter. One path towards obtaining a full-length structure is to screen for new crystallization conditions, which could generate well diffracting crystals. The construct could additionally be optimized to remove affinity tags at the end of purification route. Another strategy is to consider methods other than X-ray crystallography, such as single particle cryo-EM microscopy. The cryo-EM project is currently in the loop of improving the grids in the lab and continuously collecting and processing more data. How successful the project will become in generating high resolution structural information is yet in the future to be discovered. The aim is to determine structures of both the Pr- and Pfr state, which could be compared to provide clues about the structural mechanism of photoconversion. Excitingly, a lot of research is being focused in the direction of improving the time-resolution within the technology. Time-resolved cryo-EM could possibly be a future technique to study the full photo-cycle of phytochromes. Such research would bring us one step closer to the goal of fully understanding how plants and other organisms convert light signals into biological responses on an atomic level.

# Chapter 8

# Svensk sammanfattning

Förmågan hos olika organismer att kunna detektera och anpassa sig till de ljusförhållanden som råder i sin omgivning är avgörande för allt liv på jorden. Vissa organismer omvandlar ljuset till kemisk energi medan andra använder det för att skicka signaler i cellen. Proteiner med förmågan att uppfatta ljus kallas för fotoreceptorer. Fytokromer är en grupp av fotoreceptorer med förmågan att reagera på rött ljus och styr därigenom flertalet biologiska processer i växter, alger, svampar och bakterier. Dessa proteiner talar exempelvis om för växten om den befinner sig i skugga eller i solljus och när det är dags att blomma. Fytokromer signalerar genom att skifta mellan två olika strukturella former, där vardera form frambringar specifika typer av biologiska responser. Strukturförändringarna i proteinet orsakas av att en liten molekyl, kallad kromofor, detekterar olika våglängder av rött ljus och förmedlar signalen vidare till resten av proteinet.

Denna avhandling fokuserar på att kartlägga de första strukturella förändringar som sker i kromoforen och proteinet direkt efter det att kromoforen träffats av ljus. En metod som kan användas för att undersöka strukturen av proteiner på atomnivå är kristallografi. Genom att använda sig av en typ av tidsupplöst kristallografi, SFX, kan man dessutom följa hur olika atomer i proteinet flyttar sig över väldigt korta tidsintervall. Tack vare avancerade faciliteter (XFELs) kan man nu studera atomära förändringar på en skala av femtosekunder ($10^{15}$ s). Vi har använt dessa metoder för att studera den strukturmekanism som fytokromer använder sig av för att omvandla ljussignaler till biologiska responser. Sådan typ av information ger oss dels mer kunskap om hur all vegetation på jorden fungerar men skulle även kunna appliceras inom jordbruket, i form av förbättrade grödor.

# Acknowledgements

Time flies! I cannot believe that five years at Lundberg lab have already passed. The best thing about my PhD is without a doubt all the amazing people I got to meet. I will always remember the crazy moments we shared together!

**Sebastian**, foremost, thank you for giving me the opportunity to work on what I think has been your favorite project. You are one of the most goal-oriented people I have ever met. However, what I appreciate the most is not related to results or success, it is something that I consider far more important: I always felt that I could ask you questions, no matter how simple they were. As a teacher by heart, I hope you always keep that quality. **Richard**, thank you for being my examiner and for always being the higher power looking out for us PhD students. You also taught me that there is a sport called cricket. **Heikki**, the phytochrome expert! Thank you for sharing your knowledge and wisdom with me. You were always the steady rock at the crazy beam times.

Westenhooooffs: Coolest kids on the block! **Wejjan**, my little chihuahua. I am so glad we worked on the same project, "ty" I have learned a lot from you and you have been a great support in all categories. **Leo** <3 We came in together and we are leaving together. I am so glad that I always had your support through this journey, you're the best. Let's celebrate with champagne in Paris! **Linnea**, mama bear. Thanks for being like a big sister, always having my back. You have been missed every day since you left! **Petra E**, my phytochrome-twinne, couldn't have wished for a better partner in crime to start my PhD with. Your personality is as colorful as your hair. **Matthijs**, can one have a co-co-supervisor?! Thanks for all the endless times you came in to my office to help me with a "quick thing" which then sometimes took hours. **Joachim**, I love your laugh and your cursis in Swedish and whenever I feel down I will think of you walking around in that penguin costume. **Ann**, whoever moves in to my office space will get the corridor's best roomie. **Amke**, I tried to get in shape this year but you made it impossible with all your amazing cookies. Laser lab needs a power woman like you. **Andrea**, I recognize the willingness you have to know and understand everything you do. This will make you a great researcher!

**Michal**, I always wondered who actually buys piggelin these days, now I know. Also, it means gris-elin in Swedish. **Manoop**, good that someone is taking a close look at the DrBph photocycle! **Lidija**, I hope you find your Swedish man soon, but not only for the visum! **Laras**, good luck to the next queen of phytochromes. **Jennifer**, Thanks a lot for reading and commenting on my thesis! **Emil**, my co-founder of the "most bitter office in the lab". I don't think anyone else had to listen to me complain as much as you did, thanks for not complaining about my complaining. **Oskar**, truth is that it was never the same since you left. Thanks to both of you for the check-list..still got it!

Neutzes: **Båthis**, if there were a lab version of "who wants to be a billioner" you would always be my first choice when using the lifeline to "call a friend". **Rebecka**, all my future lunch conversations will be pale in comparison with ours. **Sarabi**, thanks for being as non-resistant to alcohol as I am… half a cider ;) **Professor Greger**, I know I am teasing you a lot but I am just jealous that you are good at absolutely everything! **Rob**, thank you for always trying to answer my provoking questions haha. **Georgia**, I am glad you showed me the coziest coffee place in town, let's have another one! **Per**, thank you for having the most awesome name, all the future Pers will be called peddan in your honor. **Swaggie**, you have got swaaag girl. **Analia, Adams, Lucija,** I am glad I got to meet you all before I finished!

Brändens: **Cecilia S**, when it comes down to it you were the thing in my list of pros and cons of doing a PhD that actually made me do it <3 Thank you for always being such a good friend and our journey is not over! **Andreas**, DJ dunge. So sad you didn't do a PhD at Lundberg because that would have been so much fuuun! **Jonathan**, I think you were one of my first students! Glad I didn't scare you off completely and I know you will do great. **Doris** and **Owens**, it is good that you spread some happiness around the lab with your laughing.

Hedfalks: **Florian**, there is too much that I could write so will keep it short: there can simply be one favorite german. **Rasmus**, thanks for the photos, great mustache. **Jessicia**, your were also not innocent in sabotaging my non-sugar diet with your very good cookies!

Katonas: **Majelitoo**, as you once said, I see a lot of you in me! Good thing we can hang out in Spain during summers, drinking some coronas and slushy margaritaaas. **Maja**, I will miss you so much. Had the best time

teaching with you and Kem021's fate lies in you hands from now on..I will pray for you ;) **Viktor**, I have never been as scared in my whole life as when we drove around in the US..haha fun times though!

Burmans: **Ylber**..regnbågen..real friendship starts with two divas thinking the other one is an even bigger diva! Thanks for being a great support this last year. **Emelie**, thanks for all the laughs! I love how you can be bossy and kind at the same time, beacuse of that you had my respect since day one. **Jens, Laura, Darius, Yosh, Lisa, Damasus and Ashish** it has been a pure pleasure meeting you all! I wish you the best of luck in the future and keep up the good beer club spirit. **Irena** I consider you a PI ;) so you have to read further down.

Höögs: **Davide**, I think you are one of the kindest and most helpful persons I have ever met, thank you for staining and freezing phytochromes with me! **Jack, Dimitra, Lisa and Katharina**, I wish we had shared floor so that I would have got to spend more time with you guys. Good luck with all your projects!

To the **Fins!** Thanks for all the fun beam times and retreats, not one of them were without a sauna..will never forget the karaoke in Japan, mostly cause I have you all on tape! To the **Americans**, thanks for a great collaboration, we could not have done it without you!

**David, Dods, Wickis, Dunis, Rhawnie, Rajjan, Stephan S, Stephan N** and **Ash** you are the golden oldies... always missed, never forgotten. So glad that our paths crossed at some point during my PhD.

**Tinna** my dear! I am so happy it was you how got the position and no one else. In my mind we are still going to Island some day. To **all the PIs**, thanks for setting a great example of how you get successful in science, you have all inspired me in some way. **Lars, Valida** and **Bruno** without you the whole lab would definitely shut down!

To my **family and friends**, thank you for always supporting me in everything I do. Thanks to you I have always been able to put things into perspective and realized what is important in life. Love you all so much and you are the ones who will still be stuck with this mess (Moi!!).

Every story comes to an end....

# Bibliography


[1] P. W. , J. De Paula, and R. Friedman, *Quanta, matter, and change: a molecular approach to physical chemistry*. Oxford University Press, 2009.

[2] Z. S.S. and Z. S.A., *Chemistry*. USA, New York: Houghton Mifflin, 6 ed., 2007.

[3] M. E. Auldridge and K. T. Forest, "Bacterial phytochromes: More than meets the light," *Critical Reviews in Biochemistry and Molecular Biology*, vol. 46, pp. 67–88, feb 2011.

[4] T. Kottke, A. Xie, D. S. Larsen, and W. D. Hoff, "Photoreceptors Take Charge: Emerging Principles for Light Sensing," *Annual Review of Biophysics*, vol. 47, no. 1, pp. 291–313, 2018.

[5] J. Dasgupta, R. R. Frontiera, K. C. Taylor, J. C. Lagarias, and R. A. Mathies, "Ultrafast excited-state isomerization in phytochrome revealed by femtosecond stimulated Raman spectroscopy.," *Proceedings of the National Academy of Sciences of the United States of America*, vol. 106, pp. 1784–9, feb 2009.

[6] M. Gauden, I. H. M. van Stokkum, J. M. Key, D. C. Lührs, R. van Grondelle, P. Hegemann, and J. T. M. Kennis, "Hydrogen-bond switching through a radical pair mechanism in a flavin-binding photoreceptor," *Proceedings of the National Academy of Sciences*, vol. 103, no. 29, pp. 10895–10900, 2006.

[7] N. C. Rockwell and J. C. Lagarias, "A brief history of phytochromes," *ChemPhysChem*, vol. 11, pp. 1172–1180, apr 2010.

[8] J. Li, G. Li, H. Wang, and X. Wang Deng, "Phytochrome signaling mechanisms.," *The arabidopsis book*, vol. 9, p. e0148, 2011.

[9] B. Karniol and R. D. Vierstra, "The pair of bacteriophytochromes from Agrobacterium tumefaciens are histidine kinases with opposing photobiological properties.," *Proceedings of the National Academy of Sciences of the United States of America*, vol. 100, no. 5, pp. 2807–2812, 2003.

[10] H. A. Borthwick, S. B. Hendricks, M. W. Parker, E. H. Toole, and V. K. Toole, "A Reversible Photoreaction Controlling Seed Germination," *Proceedings of the National Academy of Sciences*, vol. 38, pp. 662–666, aug 1952.

[11] W. L. Butler, K. H. Norris, H. W. Siegelman, and S. B. Hendricks, "DETECTION, ASSAY, AND PRELIMINARY PURIFICATION OF THE PIGMENT CONTROLLING PHOTORESPONSIVE DEVELOPMENT OF PLANTS.," *Proceedings of the National Academy of Sciences of the United States of America*, vol. 45, pp. 1703–8, dec 1959.

[12] A. Blumenstein, K. Vienken, R. Tasler, J. Purschwitz, D. Veith, N. Frankenberg-Dinkel, and R. Fischer, "The Aspergillus nidulans Phytochrome FphA Represses Sexual Development in Red Light," *Current Biology*, vol. 15, pp. 1833–1838, oct 2005.

[13] J. Hughes, T. Lamparter, F. Mittmann, E. Hartmann, W. Gärtner, A. Wilde, and T. Börner, "A prokaryotic phytochrome," *Nature*, vol. 386, pp. 663–663, apr 1997.

[14] S. J. Davis, A. V. Vener, and R. D. Vierstra, "Bacteriophytochromes: phytochrome-like photoreceptors from nonphotosynthetic eubacteria.," *Science (New York, N.Y.)*, vol. 286, pp. 2517–20, dec 1999.

[15] S. Nagano, "From photon to signal in phytochromes: similarities and differences between prokaryotic and plant phytochromes," *Journal of Plant Research*, vol. 129, pp. 123–135, mar 2016.

[16] A. Möglich, "Signal transduction in photoreceptor histidine kinases," *Protein Science*, vol. 28, no. 11, pp. 1923–1946, 2019.

[17] V. N. Pham, P. K. Kathare, and E. Huq, "Phytochromes and phytochrome interacting factors," *Plant Physiology*, vol. 176, pp. 1025–1038, feb 2018.

[18] N. C. Rockwell and J. C. Lagarias, "The structure of phytochrome: A picture is worth a thousand spectra," *Plant Cell*, vol. 18, pp. 4–14, jan 2006.

[19] F. Andel, K. C. Hasson, F. Gai, P. A. Anfinrud, and R. A. Mathies, "Femtosecond time-resolved spectroscopy of the primary photochemistry of phytochrome," *Biospectroscopy*, vol. 3, no. 6, pp. 421–433, 1997.

[20] J. J. van Thor, K. L. Ronayne, and M. Towrie, "Formation of the Early Photoproduct Lumi-R of Cyanobacterial Phytochrome Cph1 Observed by Ultrafast Mid-Infrared Spectroscopy," *Journal of the American Chemical Society*, vol. 129, pp. 126–132, jan 2007.

[21] A. Remberg, I. Lindner, T. Lamparter, J. Hughes, C. Kneip, P. Hildebrandt, S. E. Braslavsky, W. Gärtner, and K. Schaffner, "Raman spectroscopic and light-induced kinetic characterization of a recombinant phytochrome of the cyanobacterium Synechocystis," *Biochemistry*, vol. 36, pp. 13389–13395, oct 1997.

[22] J. J. van Thor, B. Borucki, W. Crielaard, H. Otto, T. Lamparter, J. Hughes, K. J. Hellingwerf, and M. P. Heyn, "Light-induced proton release and proton uptake reactions in the cyanobacterial phytochrome Cph1.," *Biochemistry*, vol. 40, no. 38, pp. 11460–11471, 2001.

[23] B. Borucki, D. von Stetten, S. Seibeck, T. Lamparter, N. Michael, M. A. Mroginski, H. Otto, D. H. Murgida, M. P. Heyn, and P. Hildebrandt, "Light-induced proton release of phytochrome is coupled to the transient deprotonation of the tetrapyrrole chromophore.," *The Journal of biological chemistry*, vol. 280, no. 40, pp. 34358–34364, 2005.

[24] J. A. Ihalainen, E. Gustavsson, L. Schroeder, S. Donnini, H. Lehtivuori, L. Isaksson, C. Thöing, V. Modi, O. Berntsson, B. Stucki-Buchli, A. Liukkonen, H. Häkkänen, E. Kalenius, S. Westenhoff, and T. Kottke, "Chromophore–protein interplay during the phytochrome photocycle revealed by step-scan ftir spectroscopy," *Journal of the American Chemical Society*, vol. 140, no. 39, pp. 12396–12404, 2018. PMID: 30183281.

[25] H. Takala, H. Lehtivuori, H. Hammarén, V. P. Hytönen, and J. A. Ihalainen, "Connection between Absorption Properties and Conformational Changes in Deinococcus radiodurans Phytochrome," *Biochemistry*, vol. 53, pp. 7076–7085, nov 2014.

[26] V. A. Sineshchekov, "Polymorphism of Phytochrome A and Its Functional Implications," in *Light Sensing in Plants*, pp. 95–102, Springer Japan, mar 2007.

[27] S. E. Braslavsky, W. Gärtner, and K. Schaffner, "Phytochrome photoconversion," *Plant, Cell and Environment*, vol. 20, pp. 700–706, jun 1997.

[28] K. Heyne, J. Herbst, D. Stehlik, B. Esteban, T. Lamparter, J. Hughes, and R. Diller, "Ultrafast dynamics of phytochrome from the cyanobacterium Synechocystis, reconstituted with phycocyanobilin and phycoerythrobilin," *Biophysical Journal*, vol. 82, pp. 1004–1016, feb 2002.

[29] W. Rudiger, F. Thummler, E. Cmiel, and S. Schneider, "Chromophore structure of the physiologically active form (Pfr) of phytochrome," *Proceedings of the National Academy of Sciences*, vol. 80, pp. 6244–6248, oct 1983.

[30] X. Yang, Z. Ren, J. Kuk, and K. Moffat, "Temperature-scan cryocrystallography reveals reaction intermediates in bacteriophytochrome," *Nature*, vol. 479, no. 7373, pp. 428–432, 2011.

[31] C. Song, G. Psakis, C. Lang, J. Mailliet, W. Gartner, J. Hughes, and J. Matysik, "Two ground state isoforms and a chromophore D-ring photoflip triggering extensive intramolecular changes in a canonical phytochrome," *Proceedings of the National Academy of Sciences*, vol. 108, pp. 3842–3847, mar 2011.

[32] E. Burgie, J. Zhang, and R. Vierstra, "Crystal Structure of Deinococcus Phytochrome in the Photoactivated State Reveals a Cascade of Structural Rearrangements during Photoconversion," *Structure*, vol. 24, pp. 448–457, mar 2016.

[33] J. Wagner, J. Brunzelle, K. Forest, and R. Vierstra, "A light-sensing knot revealed by the structure of the chromophore-binding domain of phytochrome," *Nature*, vol. 438, pp. 325–331, nov 2005.

[34] J. R. Wagner, J. Zhang, J. S. Brunzelle, R. D. Vierstra, and K. T. Forest, "High Resolution Structure of Deinococcus Bacteriophytochrome Yields New Insights into Phytochrome Architecture and Evolution," *Journal of Biological Chemistry*, vol. 282, pp. 12298–12309, apr 2007.

[35] X. Yang, J. Kuk, and K. Moffat, "Crystal structure of Pseudomonas aeruginosa bacteriophytochrome: Photoconversion and signal transduction," *Proceedings of the National Academy of Sciences*, vol. 105, pp. 14715–14720, sep 2008.

[36] L.-O. Essen, J. Mailliet, and J. Hughes, "The structure of a complete phytochrome sensory module in the Pr ground state," *Proceedings of the National Academy of Sciences*, vol. 105, pp. 14709–14714, sep 2008.

[37] H. Takala, A. Björling, O. Berntsson, H. Lehtivuori, S. Niebling, M. Hoernke, I. Kosheleva, R. Henning, A. Menzel, J. A. Ihalainen, and S. Westenhoff, "Signal amplification and transduction in phytochrome photosensors.," *Nature*, vol. 509, no. 7499, pp. 245–248, 2014.

[38] X. Yang, E. A. Stojković, W. B. Ozarowski, J. Kuk, E. Davydova, and K. Moffat, "Light Signaling Mechanism of Two Tandem Bacteriophytochromes," *Structure*, vol. 23, pp. 1179–1189, jul 2015.

[39] M. E. Auldridge, K. A. Satyshur, D. M. Anstrom, and K. T. Forest, "Structure-guided engineering enhances a phytochrome-based infrared fluorescent protein," *Journal of Biological Chemistry*, vol. 287, pp. 7000–7009, mar 2012.

[40] X. Yang, E. A. Stojković, J. Kuk, and K. Moffat, "Crystal structure of the chromophore binding domain of an unusual bacteriophytochrome, RpBphP3, reveals residues that modulate photoconversion," *Proceedings of the National Academy of Sciences of the United States of America*, vol. 104, pp. 12571–12576, jul 2007.

[41] X. Yang, J. Kuk, and K. Moffat, "Conformational differences between the Pfr and Pr states in Pseudomonas aeruginosa bacteriophytochrome," *Proceedings of the National Academy of Sciences*, vol. 106, pp. 15639–15644, sep 2009.

[42] E. Nango, A. Royant, M. Kubo, T. Nakane, C. Wickstrand, T. Kimura, T. Tanaka, K. Tono, C. Song, R. Tanaka, T. Arima, A. Yamashita, J. Kobayashi, T. Hosaka, E. Mizohata, P. Nogly, M. Sugahara, D. Nam, T. Nomura, T. Shimamura, D. Im, T. Fujiwara, Y. Yamanaka, B. Jeon, T. Nishizawa, K. Oda, M. Fukuda, R. Andersson, P. Båth, R. Dods, J. Davidsson, S. Matsuoka, S. Kawatake, M. Murata, O. Nureki, S. Owada, T. Kameshima, T. Hatsui, Y. Joti, G. Schertler, M. Yabashi, A.-N. Bondar, J. Standfuss, R. Neutze, and S. Iwata, "A three-dimensional movie of structural changes in bacteriorhodopsin.," *Science (New York, N.Y.)*, vol. 354, no. 6319, pp. 1552–1557, 2016.

[43] J. Mailliet, G. Psakis, K. Feilke, V. Sineshchekov, L. O. Essen, and J. Hughes, "Spectroscopy and a high-resolution crystal structure of Tyr263 mutants of cyanobacterial phytochrome Cph1," *Journal of Molecular Biology*, vol. 413, pp. 115–127, oct 2011.

[44] E. S. Burgie, T. Wang, A. N. Bussell, J. M. Walker, H. Li, and R. D. Vierstra, "Crystallographic and electron microscopic analyses of a bacterial phytochrome reveal local and global rearrangements during photoconversion.," *The Journal of biological chemistry*, vol. 289, no. 35, pp. 24573–24587, 2014.

[45] H. Li, J. Zhang, R. D. Vierstra, and H. Li, "Quaternary organization of a phytochrome dimer as revealed by cryoelectron microscopy.," *Proceedings of the National Academy of Sciences of the United States of America*, vol. 107, no. 24, pp. 10872–10877, 2010.

[46] A. Björling, O. Berntsson, H. Lehtivuori, H. Takala, A. J. Hughes, M. Panman, M. Hoernke, S. Niebling, L. Henry, R. Henning, I. Kosheleva, V. Chukharev, N. V. Tkachenko, A. Menzel, G. Newby, D. Khakhulin, M. Wulff, J. A. Ihalainen, and S. Westenhoff, "Structural photoactivation of a full-length bacterial phytochrome," *Science Advances*, vol. 2, no. 8, pp. e1600920–e1600920, 2016.

[47] P. Casino, L. Miguel-Romero, and A. Marina, "Visualizing autophosphorylation in histidine kinases.," *Nature communications*, vol. 5, p. 3258, 2014.

[48] L. C. Johansson, B. Stauch, A. Ishchenko, and V. Cherezov, "A Bright Future for Serial Femtosecond Crystallography with XFELs," *Trends in Biochemical Sciences*, vol. 42, pp. 749–762, sep 2017.

[49] G. Georgiou and P. Valax, "Expression of correctly folded proteins in Escherichia coli," *Current Opinion in Biotechnology*, vol. 7, no. 2, pp. 190–197, 1996.

[50] R. Vincentelli, A. Cimino, A. Geerlof, A. Kubo, Y. Satou, and C. Cambillau, "High-throughput protein expression screening and purification in Escherichia coli," *Methods*, vol. 55, pp. 65–72, sep 2011.

[51] G. L. Rosano and E. A. Ceccarelli, "Recombinant protein expression in Escherichia coli: Advances and challenges," *Frontiers in Microbiology*, vol. 5, no. APR, 2014.

[52] F. William Studier, A. H. Rosenberg, J. J. Dunn, and J. W. Dubendorff, "Use of T7 RNA polymerase to direct expression of cloned genes," *Methods in Enzymology*, 1990.

[53] K. Mukougawa, H. Kanamoto, T. Kobayashi, A. Yokota, and T. Kohchi, "Metabolic engineering to produce phytochromes with phytochromobilin, phycocyanobilin, or phycoerythrobilin chromophore in Escherichia coli," *FEBS Letters*, vol. 580, pp. 1333–1338, feb 2006.

[54] L. Deforce, K. I. Tomizawa, N. Ito, D. Farrens, P. S. Song, and M. Furuya, "In vitro assembly of apophytochrome and apophytochrome deletion mutants expressed in yeast with phycocyanobilin," *Proceedings of the National Academy of Sciences of the United States of America*, vol. 88, no. 23, pp. 10392–10396, 1991.

[55] M. S. Islam, A. Aryasomayajula, and P. R. Selvaganapathy, "A review on macroscale and microscale cell lysis methods," *Micromachines*, vol. 8, no. 3, 2017.

[56] *Strategies for Protein Purification-Handbook*. Uppsala: GE Healthcare Bio-Science AB, 2010.

[57] J. M. Berg, J. L. Tymoczko, and L. Stryer, *Biochemistry*. W.H. Freeman and Company, 6 ed., 2007.

[58] K. Wilson and J. Walker, *Principles and Techniques of Biochemistry and Molecular Biology*, vol. 7. Cambridge University Press, 2010.

[59] J. A. Bornhorst and J. J. Falke, "Purification of proteins using polyhistidine affinity tags," *Methods in Enzymology*, vol. 326, pp. 245–254, 2000.

[60] H. Block, B. Maertens, A. Spriestersbach, N. Brinker, J. Kubicek, R. Fabis, J. Labahn, and F. Schäfer, "Chapter 27 immobilized-metal affinity chromatography (imac): A review," in *Guide to Protein Purification, 2nd Edition* (R. R. Burgess and M. P. Deutscher, eds.), vol. 463 of *Methods in Enzymology*, pp. 439 – 473, Academic Press, 2009.

[61] J. M. Yoon, T. R. Hahn, M. H. Cho, J. S. Jeon, S. H. Bhoo, and Y. K. Kwon, "The PHY domain is required for conformational stability and spectral integrity of the bacteriophytochrome from Deinococcus radiodurans," *Biochemical and Biophysical Research Communications*, vol. 369, pp. 1120–1124, may 2008.

[62] G. Rhodes, *Crystallography Made Crystal Clear: A Guide for Users of Macromolecular Models*, vol. 35. Academic Press, 2006.

[63] M. A. Dessau and Y. Modis, "Protein crystallization for X-ray crystallography," *Journal of Visualized Experiments*, no. 47, 2010.

[64] R. Dods, P. Båth, D. Arnlund, K. R. Beyerlein, G. Nelson, M. Liang, R. Harimoorthy, P. Berntsen, E. Malmerberg, L. Johansson, R. Andersson, R. Bosman, S. Carbajo, E. Claesson, C. E. Conrad, P. Dahl, G. Hammarin, M. S. Hunter, C. Li, S. Lisova, D. Milathianaki, J. Robinson, C. Safari, A. Sharma, G. Williams, C. Wickstrand, O. Yefanov, J. Davidsson, D. P. DePonte, A. Barty, G. Brändén, and R. Neutze, "From Macrocrystals to Microcrystals: A Strategy for Membrane Protein Serial Crystallography," *Structure*, vol. 25, pp. 1461–1468.e2, sep 2017.

[65] T. Bergfors, "Seeds to crystals," *Journal of Structural Biology*, vol. 142, pp. 66–76, apr 2003.

[66] Jan and Drenth, *Principles of Protein X-Ray Crystallography*. Springer Science+Business Media, LLC, 3 ed., 2007.

[67] H. N. Chapman, C. Caleman, and N. Timneanu, "Diffraction before destruction," *Philosophical Transactions of the Royal Society B: Biological Sciences*, vol. 369, jul 2014.

[68] S. Boutet and M. Yabashi, "X-Ray Free Electron Lasers and Their Applications," in *X-ray Free Electron Lasers*, pp. 1–21, Cham: Springer International Publishing, 2018.

[69] R. Neutze, R. Wouts, D. van der Spoel, E. Weckert, and J. Hajdu, "Potential for biomolecular imaging with femtosecond X-ray pulses," *Nature*, vol. 406, pp. 752–757, aug 2000.

[70] H. N. Chapman, P. Fromme, A. Barty, T. A. White, R. A. Kirian, A. Aquila, M. S. Hunter, J. Schulz, D. P. DePonte, U. Weierstall, R. B. Doak, F. R. N. C. Maia, A. V. Martin, I. Schlichting, L. Lomb, N. Coppola, R. L. Shoeman, S. W. Epp, R. Hartmann, D. Rolles, A. Rudenko, L. Foucar, N. Kimmel, G. Weidenspointner, P. Holl, M. Liang, M. Barthelmess, C. Caleman, S. Boutet, M. J. Bogan, J. Krzywinski, C. Bostedt, S. Bajt, L. Gumprecht, B. Rudek, B. Erk, C. Schmidt, A. Hömke, C. Reich, D. Pietschner, L. Strüder, G. Hauser, H. Gorke, J. Ullrich, S. Herrmann, G. Schaller, F. Schopper, H. Soltau, K.-U. Kühnel, M. Messerschmidt, J. D. Bozek, S. P. Hau-Riege, M. Frank, C. Y. Hampton, R. G. Sierra, D. Starodub, G. J. Williams, J. Hajdu, N. Timneanu, M. M. Seibert, J. Andreasson, A. Rocker, O. Jönsson, M. Svenda, S. Stern, K. Nass, R. Andritschke, C.-D. Schröter, F. Krasniqi, M. Bott, K. E. Schmidt, X. Wang, I. Grotjohann, J. M. Holton, T. R. M. Barends, R. Neutze, S. Marchesini, R. Fromme, S. Schorb, D. Rupp, M. Adolph, T. Gorkhover, I. Andersson, H. Hirsemann, G. Potdevin, H. Graafsma, B. Nilsson, and J. C. H. Spence, "Femtosecond X-ray protein nanocrystallography.," *Nature*, vol. 470, pp. 73–7, feb 2011.

[71] K. Nass, L. Foucar, T. R. Barends, E. Hartmann, S. Botha, R. L. Shoeman, R. B. Doak, R. Alonso-Mori, A. Aquila, S. Bajt, A. Barty, R. Bean, K. R. Beyerlein, M. Bublitz, N. Drachmann, J. Gregersen, H. O. Jönsson, W. Kabsch, S. Kassemeyer, J. E. Koglin, M. Krumrey, D. Mattle, M. Messerschmidt, P. Nissen, L. Reinhard, O. Sitsel, D. Sokaras, G. J. Williams, S. Hau-Riege, N. Timneanu, C. Caleman, H. N. Chapman, S. Boutet, and I. Schlichting, "Indications of radiation damage in ferredoxin microcrystals using high-intensity X-FEL beams," *Journal of Synchrotron Radiation*, vol. 22, pp. 225–238, mar 2015.

[72] D. P. DePonte, U. Weierstall, K. Schmidt, J. Warner, D. Starodub, J. C. Spence, and R. B. Doak, "Gas dynamic virtual nozzle for generation of microscopic droplet streams," *Journal of Physics D: Applied Physics*, vol. 41, oct 2008.

[73] M. S. Hunter, B. Segelke, M. Messerschmidt, G. J. Williams, N. A. Zatsepin, A. Barty, W. Henry Benner, D. B. Carlson, M. Coleman, A. Graf, S. P. Hau-Riege, T. Pardini, M. Marvin Seibert, J. Evans, S. Boutet, and M. Frank, "Fixed-target protein serial microcrystallography with an X-ray free electron laser," *Scientific Reports*, vol. 4, aug 2014.

[74] C. Mueller, A. Marx, S. W. Epp, Y. Zhong, A. Kuo, A. R. Balo, J. Soman, F. Schotte, H. T. Lemke, R. L. Owen, E. F. Pai, A. R. Pearson, J. S. Olson, P. A. Anfinrud, O. P. Ernst, and R. J. Miller, "Fixed target matrix for femtosecond time-resolved and in situ serial micro-crystallography," *Structural Dynamics*, vol. 2, sep 2015.

[75] F. D. Fuller, S. Gul, R. Chatterjee, E. Sethe Burgie, I. D. Young, H. Lebrette, V. Srinivas, A. S. Brewster, T. Michels-Clark, J. A. Clinger, B. Andi, M. Ibrahim, E. Pastor, C. De Lichtenberg, R. Hussein, C. J. Pollock, M. Zhang, C. A. Stan, T. Kroll, T. Fransson, C. Weninger, M. Kubin, P. Aller, L. Lassalle, P. Bräuer, M. D. Miller, M. Amin, S. Koroidov, C. G. Roessler, M. Allaire, R. G. Sierra, P. T. Docker, J. M. Glownia, S. Nelson, J. E. Koglin, D. Zhu, M. Chollet, S. Song, H. Lemke, M. Liang, D. Sokaras, R. Alonso-Mori, A. Zouni, J. Messinger, U. Bergmann, A. K. Boal, J. Martin Bollinger, C. Krebs, M. Högbom, G. N. Phillips, R. D. Vierstra, N. K. Sauter, A. M. Orville, J. Kern, V. K. Yachandra, and J. Yano, "Drop-on-demand sample delivery for studying biocatalysts in action at X-ray free-electron lasers," *Nature Methods*, vol. 14, pp. 443–449, feb 2017.

[76] C. G. Roessler, R. Agarwal, M. Allaire, R. Alonso-Mori, B. Andi, J. F. Bachega, M. Bommer, A. S. Brewster, M. C. Browne, R. Chatterjee, E. Cho, A. E. Cohen, M. Cowan, S. Datwani, V. L. Davidson, J. Defever, B. Eaton, R. Ellson, Y. Feng, L. P. Ghislain, J. M. Glownia, G. Han, J. Hattne, J. Hellmich, A. Héroux, M. Ibrahim, J. Kern, A. Kuczewski, H. T. Lemke, P. Liu, L. Majlof, W. M. McClintock, S. Myers, S. Nelsen, J. Olechno, A. M. Orville, N. K. Sauter, A. S. Soares, S. M. Soltis, H. Song, R. G. Stearns, R. Tran, Y. Tsai, M. Uervirojnangkoorn, C. M. Wilmot, V. Yachandra, J. Yano, E. T. Yukl, D. Zhu, and A. Zouni, "Acoustic Injectors for Drop-On-Demand Serial Femtosecond Crystallography," *Structure*, vol. 24, pp. 631–640, apr 2016.

[77] U. Weierstall, D. James, C. Wang, T. A. White, D. Wang, W. Liu, J. C. Spence, R. Bruce Doak, G. Nelson, P. Fromme, R. Fromme, I. Grotjohann, C. Kupitz, N. A. Zatsepin, H. Liu, S. Basu, D. Wacker, G. Won Han, V. Katritch, S. Boutet, M. Messerschmidt, G. J. Williams, J. E. Koglin, M. Marvin Seibert, M. Klinker, C. Gati, R. L. Shoeman, A. Barty, H. N. Chapman, R. A. Kirian, K. R. Beyerlein, R. C. Stevens, D. Li, S. T. Shah, N. Howe, M. Caffrey, and V. Cherezov, "Lipidic cubic phase injector facilitates membrane protein serial femtosecond crystallography," *Nature Communications*, vol. 5, feb 2014.

[78] W. Liu, A. Ishchenko, and V. Cherezov, "Preparation of microcrystals in lipidic cubic phase for serial femtosecond crystallography," *Nature Protocols*, vol. 9, no. 9, pp. 2123–2134, 2014.

[79] M. Sugahara, E. Mizohata, E. Nango, M. Suzuki, T. Tanaka, T. Masuda, R. Tanaka, T. Shimamura, Y. Tanaka, C. Suno, K. Ihara, D. Pan, K. Kakinouchi, S. Sugiyama, M. Murata, T. Inoue, K. Tono, C. Song, J. Park, T. Kameshima, T. Hatsui, Y. Joti, M. Yabashi, and S. Iwata, "Grease matrix as a versatile carrier of proteins for serial crystallography," *Nature Methods*, vol. 12, pp. 61–63, jan 2014.

[80] M. Sugahara, T. Nakane, T. Masuda, M. Suzuki, S. Inoue, C. Song, R. Tanaka, T. Nakatsu, E. Mizohata, F. Yumoto, K. Tono, Y. Joti, T. Kameshima, T. Hatsui, M. Yabashi, O. Nureki, K. Numata, E. Nango, and S. Iwata, "Hydroxyethyl cellulose matrix applied to serial crystallography," *Scientific Reports*, vol. 7, dec 2017.

[81] J. Coe and P. Fromme, "Serial femtosecond crystallography opens new avenues for Structural Biology.," *Protein and peptide letters*, vol. 23, no. 3, pp. 255–72, 2016.

[82] C. Kupitz, S. Basu, I. Grotjohann, R. Fromme, N. A. Zatsepin, K. N. Rendek, M. S. Hunter, R. L. Shoeman, T. A. White, D. Wang, D. James, J. H. Yang, D. E. Cobb, B. Reeder, R. G. Sierra, H. Liu, A. Barty, A. L. Aquila, D. Deponte, R. A. Kirian, S. Bari, J. J. Bergkamp, K. R. Beyerlein, M. J. Bogan, C. Caleman, T. C. Chao, C. E. Conrad, K. M. Davis, H. Fleckenstein, L. Galli, S. P. Hau-Riege, S. Kassemeyer, H. Laksmono, M. Liang, L. Lomb, S. Marchesini, A. V. Martin, M. Messerschmidt, D. Milathianaki, K. Nass, A. Ros, S. Roy-Chowdhury, K. Schmidt, M. Seibert, J. Steinbrener, F. Stellato, L. Yan, C. Yoon, T. A. Moore, A. L. Moore, Y. Pushkar, G. J. Williams, S. Boutet, R. B. Doak, U. Weierstall, M. Frank, H. N. Chapman, J. C. Spence, and P. Fromme, "Serial time-resolved crystallography of photosystem II using a femtosecond X-ray laser," *Nature*, vol. 513, no. 7517, pp. 261–265, 2014.

[83] J. Tenboer, S. Basu, N. Zatsepin, K. Pande, D. Milathianaki, M. Frank, M. Hunter, S. Boutet, G. J. Williams, J. E. Koglin, D. Oberthuer, M. Heymann, C. Kupitz, C. Conrad, J. Coe, S. Roy-Chowdhury, U. Weierstall, D. James, D. Wang, T. Grant, A. Barty, O. Yefanov, J. Scales, C. Gati, C. Seuring, V. Srajer, R. Henning, P. Schwander, R. Fromme, A. Ourmazd, K. Moffat, J. J. Van Thor, J. C. Spence, P. Fromme, H. N. Chapman, and M. Schmidt, "Time-resolved serial crystallography captures high-resolution intermediates of photoactive yellow protein," *Science*, vol. 346, pp. 1242–1246, dec 2014.

[84] C. Kupitz, J. L. Olmos, M. Holl, L. Tremblay, K. Pande, S. Pandey, D. Oberthür, M. Hunter, M. Liang, A. Aquila, J. Tenboer, G. Calvey, A. Katz, Y. Chen, M. O. Wiedorn, J. Knoska, A. Meents, V. Majriani, T. Norwood, I. Poudyal, T. Grant, M. D. Miller, W. Xu, A. Tolstikova, A. Morgan, M. Metz, J. M. Martín-García, J. D. Zook, S. Roy-Chowdhury, J. Coe, N. Nagaratnam, D. Meza, R. Fromme, S. Basu, M. Frank, T. White, A. Barty, S. Bajt, O. Yefanov, H. N. Chapman, N. Zatsepin, G. Nelson, U. Weierstall, J. Spence, P. Schwander, L. Pollack, P. Fromme, A. Ourmazd, G. N. Phillips, and M. Schmidt, "Structural enzymology using X-ray free electron lasers," *Structural Dynamics*, vol. 4, jul 2017.

[85] S. Owada, K. Nakajima, T. Togashi, T. Katayama, H. Yumoto, H. Ohashi, and M. Yabashi, "Arrival timing diagnostics at a soft x-ray free-electron laser beamline of SACLA BL1," *Journal of Synchrotron Radiation*, vol. 26, pp. 887–890, may 2019.

[86] K. Nakajima, Y. Joti, T. Katayama, S. Owada, T. Togashi, T. Abe, T. Kameshima, K. Okada, T. Sugimoto, M. Yamaga, T. Hatsui, and M. Yabashi, "Software for the data analysis of the arrival-timing monitor at SACLA," *Journal of Synchrotron Radiation*, vol. 25, pp. 592–603, mar 2018.

[87] T. Katayama, S. Owada, T. Togashi, K. Ogawa, P. Karvinen, I. Vartiainen, A. Eronen, C. David, T. Sato, K. Nakajima, Y. Joti, H. Yumoto, H. Ohashi, and M. Yabashi, "A beam branching method for timing and spectral characterization of hard X-ray free-electron lasers," *Structural Dynamics*, vol. 3, p. 034301, may 2016.

[88] P. Hart, S. Boutet, G. Carini, A. Dragone, B. Duda, D. Freytag, G. Haller, R. Herbst, S. Herrmann, C. Kenney, J. Morse, M. Nordby, J. Pines, N. Van Bakel, M. Weaver, and G. Williams, "The Cornell-SLAC pixel array detector at LCLS," in *IEEE Nuclear Science Symposium Conference Record*, pp. 538–541, 2012.

[89] T. Kameshima, S. Ono, T. Kudo, K. Ozaki, Y. Kirihara, K. Kobayashi, Y. Inubushi, M. Yabashi, T. Horigome, A. Holland, K. Holland, D. Burt, H. Murao, and T. Hatsui, "Development of an X-ray pixel detector with multi-port charge-coupled device for X-ray free-electron laser experiments," *Review of Scientific Instruments*, vol. 85, no. 3, 2014.

[90] A. Barty, R. Kirian, F. Maia, M. Hantke, C. Yoon, T. White, and H. Chapman, "Cheetah: Software for high-throughput reduction and analysis of serial femtosecond x-ray diffraction data," *Journal of Applied Crystallography*, vol. 47, no. 3, pp. 1118–1131, 2014.

[91] T. G. G. Battye, L. Kontogiannis, O. Johnson, H. R. Powell, and A. G. Leslie, "iMOSFLM: A new graphical interface for diffraction-image processing with MOSFLM," *Acta Crystallographica Section D: Biological Crystallography*, vol. 67, pp. 271–281, apr 2011.

[92] A. G. W. Leslie, "The integration of macromolecular diffraction data," *Acta Crystallographica Section D*, vol. 62, pp. 48–57, jan 2006.

[93] W. Kabsch, B. A. T., D. K., K. P. A., D. K., M. S., R. R. B. G., E. P., F. S., W. K., K. W., K. W., K. W., K. W., K. P., and W. M. S., "XDS," *Acta Crystallographica Section D Biological Crystallography*, vol. 66, pp. 125–132, feb 2010.

[94] G. J. Kleywegt, "Validation of protein crystal structures," *Acta Crystallographica Section D: Biological Crystallography*, vol. 56, no. 3, pp. 249–265, 2000.

[95] L. Potterton, J. Agirre, C. Ballard, K. Cowtan, E. Dodson, P. R. Evans, H. T. Jenkins, R. Keegan, E. Krissinel, K. Stevenson, A. Lebedev, S. J. McNicholas, R. A. Nicholls, M. Noble, N. S. Pannu, C. Roth, G. Sheldrick, P. Skubak, J. Turkenburg, V. Uski, F. Von Delft, D. Waterman, K. Wilson, M. Winn, and M. Wojdyr, "CCP 4 i 2: The new graphical user interface to the CCP 4 program suite," *Acta Crystallographica Section D: Structural Biology*, vol. 74, pp. 68–84, 2018.

[96] P. D. Adams, P. V. Afonine, G. Bunkóczi, V. B. Chen, I. W. Davis, N. Echols, J. J. Headd, L. W. Hung, G. J. Kapral, R. W. Grosse-Kunstleve, A. J. McCoy, N. W. Moriarty, R. Oeffner, R. J. Read, D. C. Richardson, J. S. Richardson, T. C. Terwilliger, and P. H. Zwart, "PHENIX: A comprehensive Python-based system for macromolecular structure solution," *Acta Crystallographica Section D: Biological Crystallography*, vol. 66, no. 2, pp. 213–221, 2010.

[97] T. A. White, V. Mariani, W. Brehm, O. Yefanov, A. Barty, K. R. Beyerlein, F. Chervinskii, L. Galli, C. Gati, T. Nakane, A. Tolstikova, K. Yamashita, C. H. Yoon, K. Diederichs, H. N. Chapman, and IUCr, "Recent developments in CrystFEL," *Journal of Applied Crystallography*, vol. 49, pp. 680–689, apr 2016.

[98] R. A. Kirian, X. Wang, U. Weierstall, K. E. Schmidt, J. C. H. Spence, M. Hunter, P. Fromme, T. White, H. N. Chapman, and J. Holton, "Femtosecond protein nanocrystallography—data analysis methods," *Optics Express*, vol. 18, p. 5713, mar 2010.

[99] T. A. White, R. A. Kirian, A. V. Martin, A. Aquila, K. Nass, A. Barty, and H. N. Chapman, "CrystFEL: A software suite for snapshot serial crystallography," *Journal of Applied Crystallography*, vol. 45, pp. 335–341, feb 2012.

[100] Z. Ren, B. Perman, V. Šrajer, T.-Y. Teng, C. Pradervand, D. Bourgeois, F. Schotte, T. Ursby, R. Kort, M. Wulff, and K. Moffat, "A Molecular Movie at 1.8 Å Resolution Displays the Photocycle of Photoactive Yellow Protein, a Eubacterial Blue-Light Receptor, from Nanoseconds to Seconds <sup>†</sup>," *Biochemistry*, vol. 40, pp. 13788–13801, nov 2001.

[101] T. Ursby and D. Bourgeois, "Improved Estimation of Structure-Factor Difference Amplitudes-from Poorly Accurate Data," *Acta Crystallographica Section A Foundations of Crystallography*, vol. 53, pp. 564–575, sep 1997.

[102] P. Emsley, B. Lohkamp, W. G. Scott, and K. Cowtan, "Features and development of Coot," *Acta Crystallographica Section D: Biological Crystallography*, vol. 66, no. 4, pp. 486–501, 2010.

[103] C. Wickstrand, G. Katona, T. Nakane, P. Nogly, J. Standfuss, E. Nango, and R. Neutze, "A tool for visualizing protein motions in time-resolved crystallography," *Submitted Manuscript*, 2020.

[104] K. C. Toh, E. A. Stojković, I. H. Van Stokkum, K. Moffat, and J. T. Kennis, "Proton-transfer and hydrogen-bond interactions determine fluorescence quantum yield and photochemical efficiency of bacteriophytochrome," *Proceedings of the National Academy of Sciences of the United States of America*, vol. 107, pp. 9170–9175, may 2010.

[105] C. Schumann, R. Groß, N. Michael, T. Lamparter, and R. Diller, "Sub-picosecond mid-infrared spectroscopy of phytochrome Agp1 from Agrobacterium tumefaciens," *ChemPhysChem*, vol. 8, pp. 1657–1663, aug 2007.

[106] S. Pandey, R. Bean, T. Sato, I. Poudyal, J. Bielecki, J. Cruz Villarreal, O. Yefanov, V. Mariani, T. A. White, C. Kupitz, M. Hunter, M. H. Abdellatif, S. Bajt, V. Bondar, A. Echelmeier, D. Doppler, M. Emons, M. Frank, R. Fromme, Y. Gevorkov, G. Giovanetti, M. Jiang, D. Kim, Y. Kim, H. Kirkwood, A. Klimovskaia, J. Knoska, F. H. Koua, R. Letrun, S. Lisova, L. Maia,

V. Mazalova, D. Meza, T. Michelat, A. Ourmazd, G. Palmer, M. Ramilli, R. Schubert, P. Schwander, A. Silenzi, J. Sztuk-Dambietz, A. Tolstikova, H. N. Chapman, A. Ros, A. Barty, P. Fromme, A. P. Mancuso, and M. Schmidt, "Time-resolved serial femtosecond crystallography at the European XFEL," *Nature Methods*, vol. 17, pp. 73–78, jan 2020.

[107] K. Pande, C. D. M. Hutchison, G. Groenhof, A. Aquila, J. S. Robinson, J. Tenboer, S. Basu, S. Boutet, D. P. DePonte, M. Liang, T. A. White, N. A. Zatsepin, O. Yefanov, D. Morozov, D. Oberthuer, C. Gati, G. Subramanian, D. James, Y. Zhao, J. Koralek, J. Brayshaw, C. Kupitz, C. Conrad, S. Roy-Chowdhury, J. D. Coe, M. Metz, P. L. Xavier, T. D. Grant, J. E. Koglin, G. Ketawala, R. Fromme, V. rajer, R. Henning, J. C. H. Spence, A. Ourmazd, P. Schwander, U. Weierstall, M. Frank, P. Fromme, A. Barty, H. N. Chapman, K. Moffat, J. J. van Thor, and M. Schmidt, "Femtosecond structural dynamics drives the trans/cis isomerization in photoactive yellow protein," *Science*, vol. 352, pp. 725–729, may 2016.

[108] J. R. Wagner, J. Zhang, D. von Stetten, M. Günther, D. H. Murgida, M. A. Mroginski, J. M. Walker, K. T. Forest, P. Hildebrandt, and R. D. Vierstra, "Mutational Analysis of Deinococcus radiodurans Bacteriophytochrome Reveals Key Amino Acids Necessary for the Photochromicity and Proton Exchange Cycle of Phytochromes," *Journal of Biological Chemistry*, vol. 283, pp. 12212–12226, may 2008.

[109] A. J. Fischer and J. C. Lagarias, "Harnessing phytochrome's glowing potential," *Proceedings of the National Academy of Sciences of the United States of America*, vol. 101, pp. 17334–17339, dec 2004.

[110] V. Sineshchekov, J. Mailliet, G. Psakis, K. Feilke, J. Kopycki, M. Zeidler, L. O. Essen, and J. Hughes, "Tyrosine 263 in cyanobacterial phytochrome Cph1 optimizes photochemistry at the prelumi-R $\rightarrow$ lumi-R step," *Photochemistry and Photobiology*, vol. 90, pp. 786–795, mar 2014.

[111] Y. Yang, M. Linke, T. von Haimberger, R. Matute, L. González, P. Schmieder, and K. Heyne, "Active and silent chromophore isoforms for phytochrome Pr photoisomerization: An alternative evolutionary strategy to optimize photoreaction quantum yields," *Structural Dynamics*, vol. 1, jan 2014.

[112] H. M. Berman, J. Westbrook, Z. Feng, G. Gilliland, T. N. Bhat, H. Weissig, I. N. Shindyalov, and P. E. Bourne, "The Protein Data Bank," *Nucleic Acids Research*, vol. 28, pp. 235–242, 01 2000.

[113] "Worldwide Protein Data Bank biocuration supporting open access to high-quality 3D structural biology data. (2020, February 24). Retrieved from https://www.ncbi.nlm.nih.gov/pmc/articles/PMC5804564/,"

[114] X. Chen, B. Zheng, and H. Liu, "Optical and digital microscopic imaging techniques and applications in pathology," *Analytical Cellular Pathology*, vol. 34, no. 1-2, pp. 5–18, 2011.

[115] D. J. De Rosier and A. Klug, "Reconstruction of three dimensional structures from electron micrographs," *Nature*, vol. 217, no. 5124, pp. 130–134, 1968.

[116] Y. Cheng, "Single-particle Cryo-EM at crystallographic resolution," *Cell*, vol. 161, pp. 450–457, apr 2015.

[117] R. M. Glaeser, "Proteins, interfaces, and cryo-EM grids," *Current Opinion in Colloid and Interface Science*, vol. 34, pp. 1–8, mar 2018.

[118] Y. Cheng, "Single-particle cryo-EM-How did it get here and where will it go," *Science*, vol. 361, pp. 876–880, aug 2018.

[119] R. Henderson, "The Potential and Limitations of Neutrons, Electrons and X-Rays for Atomic Resolution Microscopy of Unstained Biological Molecules," *Quarterly Reviews of Biophysics*, vol. 28, no. 2, pp. 171–193, 1995.

[120] G. McMullan, A. R. Faruqi, and R. Henderson, "Direct Electron Detectors," *Methods in Enzymology*, vol. 579, pp. 1–17, jan 2016.

[121] D. Bhella, "Cryo-electron microscopy: an introduction to the technique, and considerations when working to establish a national facility," *Biophysical Reviews*, vol. 11, pp. 515–519, aug 2019.

[122] I. Drulyte, R. M. Johnson, E. L. Hesketh, D. L. Hurdiss, C. A. Scarff, S. A. Porav, N. A. Ranson, S. P. Muench, and R. F. Thompson, "Approaches to altering particle distributions in cryo-electron microscopy sample preparation," *Acta Crystallographica Section D: Structural Biology*, vol. 74, pp. 560–571, jun 2018.

[123] " Science Learning Hub – Pokapū Akoranga Pūtaiao. (2019). Preparing samples for the electron microscope. Retrieved from https://www.sciencelearn.org.nz/resources/500-preparing-samples-for-the-electron-microscope."

[124] M. Ohi, Y. Li, Y. Cheng, and T. Walz, "Negative staining and image classification - Powerful tools in modern electron microscopy," *Biological Procedures Online*, vol. 6, pp. 23–34, jan 2004.

[125] C. A. Scarff, M. J. Fuller, R. F. Thompson, and M. G. Iadaza, "Variations on negative stain electron microscopy methods: Tools for tackling challenging systems," *Journal of Visualized Experiments*, vol. 2018, feb 2018.

[126] J. Dubochet, M. Adrian, J.-J. Chang, J.-C. Homo, J. Lepault, A. W. McDowall, and P. Schultz, "Cryo-electron microscopy of vitrified specimens," *Quarterly Reviews of Biophysics*, vol. 21, no. 2, p. 129–228, 1988.

[127] M. J. Dobro, L. A. Melanson, G. J. Jensen, and A. W. McDowall, "Chapter three - plunge freezing for electron cryomicroscopy," in *Cryo-EM Part A Sample Preparation and Data Collection* (G. J. Jensen, ed.), vol. 481 of *Methods in Enzymology*, pp. 63 – 82, Academic Press, 2010.

[128] R. M. Glaeser, "How good can cryo-EM become?," *Nature Methods*, vol. 13, pp. 28–32, dec 2015.

[129] D. Lyumkis, "Challenges and opportunities in cryo-EM single-particle analysis," *Journal of Biological Chemistry*, vol. 294, no. 13, pp. 5181–5197, 2019.